

THE DYNAMICAL EVOLUTION OF H II REGIONS— Recent Theoretical Developments

Harold W. Yorke

Universitäts-Sternwarte Göttingen, D-3400 Göttingen, Federal Republic
of Germany

1. INTRODUCTION

The theoretical study of H II regions is a field now almost 50 years old. Investigations of how H II regions form and evolve rely on skills and understanding from several areas of astrophysics. The overall structure of the interstellar medium and, in particular, the conditions in molecular clouds where massive stars form are crucial parameters. Details of star formation, stellar structure and atmospheres, stellar evolution and mass loss, microphysical processes, hydrodynamics, radiation transfer, and numerical methods are all important ingredients for theoretical studies. Progress in piecing together the sequence of events during the evolution of H II regions and in determining the relative importance of various competing effects has depended on both theoretical and observational advances in these related fields.

The following review is intended to be selectively comprehensive rather than exhaustive. References are often made to recent review articles, the published proceedings of conferences, and comprehensive monographs instead of strictly to original sources. Emphasis has been placed on theoretical studies and the more global aspects of interpretations of observations, rather than on the observations themselves or on detailed models of individual sources.

We begin with a short introduction on some of the relevant aspects of stellar evolution and the structure of the interstellar medium. In Section 2 we briefly describe the equations to be solved and possible approximations.

After discussing the “classical” theory of H II region evolution, the results of recent investigations of a nonclassical nature are then reviewed. In the final section, current observations are compared with theory.

1.1 *Emission Nebulae: Interaction Between the Interstellar Medium and Evolving Stars*

The interstellar medium in a galaxy, a mixture of gas and dust permeated by magnetic fields and energetic cosmic-ray particles, is known to be highly inhomogeneous with respect to density and temperature. It is customary to think of this as a mixture of “phases” (see Table 1). The exact divisions and subdivisions into the various components and their estimated relative abundances in the Galaxy vary from author to author. Neutral material [H I clouds and molecular clouds with clumpy substructure (13, 75, 123)] is embedded in an ambient medium that is an inhomogeneous mixture of warm ($T \sim 10^4$ K), mainly photoionized gas and a hot ($T \geq 10^6$ K), tenuous medium [e.g. McCray & Snow (110)]. The warm component consists of emission nebulae on the one hand and an extended low-density H II region (32, 112, 172), or “warm intercloud medium,” on the other. Actually, this subdivision is somewhat arbitrary and depends on the observability at the characteristic wavelengths.

Emission nebulae are classified according to the nature of their ionizing sources and to some degree the origin of the material being ionized (see Table 1). The suggestion by Shklovskij (147) that planetary nebulae (PN) can form following the ejection of the extended envelope of a red supergiant, which is subsequently ionized by the hot, degenerate stellar core, is generally accepted [e.g. Kaler (77)]. Other possible “ejection” nebulae can occur, since not all PN nuclei are white dwarfs. Some ring nebulae around Wolf-Rayet (W-R) stars, for example, may be a consequence of the W-R formation process during which the envelope of a massive star is ejected, leaving behind a hot, helium-burning core (e.g. 20, 31, 109). It is not clear exactly how and when this occurs and whether or not this is the normal evolutionary sequence for all O stars; there may be more than one formation mechanism for W-R stars (29, 36, 37, 97). Symbiotic stars are also known to be the exciting sources of emission nebulae, the material of which is thought to have originated from one member, or in some sense both members, of a close binary pair experiencing mass transfer (e.g. 52).

Finally, bipolar (biconical) nebulae are generally interpreted as emission nebulae, the material of which originates in a collimated mass-loss (or ejection) phenomenon. Examples of bipolar nebulae that are PN, pre-PN, or associated with very young objects in star-forming regions are known [e.g. Elsässer (47), Lada (85)].

In what follows we designate such emission nebulae E-type (ejection

Table 1 Phases of interstellar matter (cf. 39)

		Interstellar matter (gas + dust)					
		Neutral components		Ionized components			
		Mostly molecular	Mostly atomic	Warm ($T \sim 10^4$ K) photoionized component		Hot ($T \geq 10^5$ K) collisionally ionized component	
		Molecular clouds	H I clouds	Extended, low-density H II region (inter- cloud medium)	H II regions and related nebulae ^b	Supernova remnants, "coronal gas"	
Relative abundance in disk	By mass	0.4	0.4	0.2	$\ll 1$	10^{-3}	
	By volume	10^{-4}	0.01	0.5	$\ll 1$	0.5	
$\langle n \rangle^a$	[cm^{-3}]	10^3	10	0.1	10	$< 10^{-3}$	
$\langle T \rangle^a$	[K]	10	50	5000	10^4	10^6	
Source of photoionization	-----			UV starlight, X-ray background (+ cosmic rays)	Young, early- type stars (single or in associations)	Evolved objects (white dwarfs, W-R stars)	
Source of ionized material	-----			Evolved, rarified photoionized nebulae, cooled supernova remnants, and stellar wind bubbles	Neutral clouds	Mass loss from newly formed stars	Mass loss from evolving star
					S-type	E-type	

^a The mean densities $\langle n \rangle$ and temperatures $\langle T \rangle$ are meant to be illustrative; large variations, especially of density, can be expected. The numbers given reflect to some extent the author's personal bias.

^b Emission nebulae are subdivided into E-types and S-types (see text).

type) to emphasize their similarity resulting from their common mode of origin (intense mass loss). H II regions resulting from ionization of the ambient medium surrounding early-type stars [first considered by Strömgren (162)] are referred to as S-type. Hybrid types of emission nebulae are possible in which the ionized material originates partly from mass loss and partly from ambient neutral material overtaken by an ionization front (I-front). Varying mass-loss rates and ultraviolet ionizing luminosities may result in one type changing into another. Such changes, as well as phase transitions in the ambient interstellar medium, are intimately related to details of stellar evolution.

1.2 *Time Scales of Stellar Evolution*

Important domains in the age versus zero-age main sequence (ZAMS) mass of evolving stars are shown in Figure 1. Numerical calculations (e.g. 16, 88, 89, 191, 201) indicate that for the first 10^5 yr a newly formed hydrostatic core (“protostar”) continues to accrete material from the protostellar envelope while it contracts to hydrogen-burning temperatures and densities. Higher mass protostars contract faster than those of lower mass, and for protostars more massive than $3\text{--}5 M_{\odot}$, hydrogen burning begins (curve 2) before the accretion phase ends (curve 3). During the accretion phase the accreting protostar or accreting hydrogen-burning star is completely obscured optically ($A_v \gg 1$) but can be observed as an IR source because of the radiation of the heated circumstellar dust cocoon (17, 198). One speaks of a cocoon star or cocoon protostar depending on whether the central object is pre-main sequence or hydrogen burning. Probably all of the luminous infrared “protostellar candidates” discussed by Wynn-Williams (193) are cocoon stars rather than protostars, because the pre-main sequence phase for massive stars is so short lived. After the accretion phase the protostellar cloud has been either accreted or dispersed, and depending on how deeply embedded within the molecular cloud the protostellar collapse was initiated, the central core may then be optically visible. Low-mass stars ($M < 3 M_{\odot}$) may become visible optically long before they reach the main sequence (curve 1). YY Orionis and T Tauri are good candidates for such objects (16, 17).

During advanced stages of the accretion phase, ultracompact H II regions can form if the stars are sufficiently massive. Fossil accretion disks may still exist at this time, and mass-loss activity can occur concurrently. For the sake of discussion we have set a ZAMS lower mass limit of $8 M_{\odot}$ (spectral type B3 or B4) for the exciting stars of H II regions in Figure 1. The same mass limit was used to separate those stars that are supernova progenitors [producing an expanding supernova remnant (SNR)] from those stars that are able to lose sufficient mass and evolve into white dwarfs

(either with or without an observable planetary nebula). One-million-year-old supernova remnants would not be distinguishable as such (curve 6), whereas planetary nebulae have a typical observable lifetime of several $\times 10^4$ yr at most. This corresponds to a domain of existence in Figure 1 that is less than the thickness of curve 5.

Stellar evolution tracks in Figure 1 are by definition horizontal lines from left to right. A vertical line at say, $t = t_0$ shows the mixture of evolutionary phases and domains encompassed at a time t_0 after a star formation "flash" (delta-function star formation rate) in a molecular

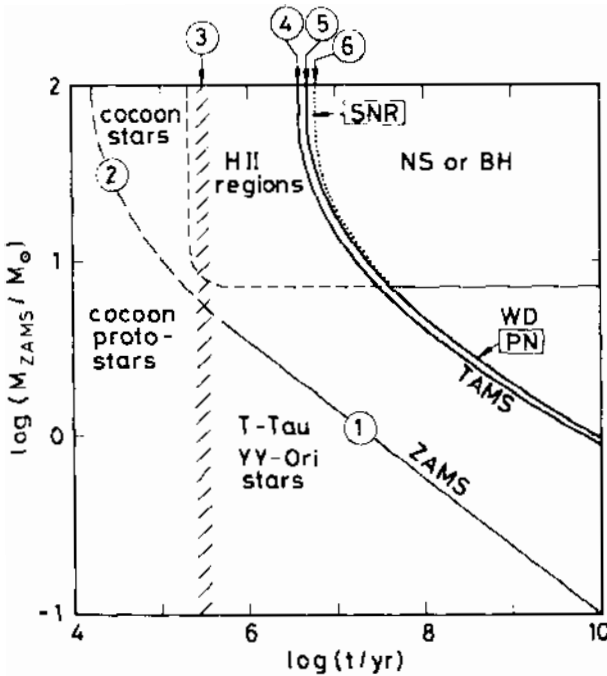


Figure 1 Important domains in the mass versus age plane during stellar evolution. (1.) Pre-main sequence evolution time = Kelvin-Helmholtz contraction time. Stars are close to the zero-age main sequence (ZAMS). (2.) Pre-hydrogen-burning evolution time for an accreting protostar (schematic; depends on the accretion time scale and the time scale for angular momentum transport). (3.) Accretion time scale for protostellar clouds with initial densities $n \approx 10^5 \text{ cm}^{-3}$. (4.) End of core hydrogen burning. (5.) End of nuclear burning. (6.) 10^6 yr after a supernova explosion. At this time a supernova remnant should not be recognizable as such. Evolutionary tracks compiled by Cox & Giuli (34) without mass loss were used for curves 1, 4, and 5. Mass loss modifies the exact locations of curves 4 and 5 (30). Curve 2 has been estimated from a number of sources (88, 194, 195), including unpublished computations by the author. Abbreviations are as follows: NS, neutron star; BH, black hole; WD, white dwarf; SNR, supernova remnant; PN, planetary nebula.

cloud. Such perfect “flashes” are unrealistic because even if collapse and fragmentation of molecular clouds could be initialized simultaneously in all parts, inherent density fluctuations will produce scatter in the free-fall times and accretion time scales of the protostellar fragments. Without entering into the controversy about the longevity of molecular clouds and whether or not they exist in interarm regions (e.g. 19, 90, 143, 145, 154, 175, 199), we remark that at least OB star-producing molecular clouds [type II clouds according to the classification scheme of Stenholm (160)] are not found between spiral arms and therefore should be short lived (several $\times 10^7$ yr). The minimum scatter of ages in a stellar cluster can be expected to be of the order of the free-fall time of the parent molecular cloud

$$[t_{\text{ff}} \simeq 10^6 \text{ yr } (n_{\text{H}_2}/10^3 \text{ cm}^{-3})^{-1/2}].$$

In this sense, Figure 1 illustrates some of the difficulties encountered in the study of the evolution of H II regions. OB stars rarely if ever form individually, and their respective H II regions should combine and interact as the nebulae and their exciting stars evolve. After several million years the most massive stars approach the end of main sequence hydrogen burning. Even if the main sequence winds of these stars previously had negligible influence on the global evolution of their H II region(s), late nuclear-burning phases are almost certainly accompanied by intense mass loss (e.g. 27, 30, 33, 44). As discussed at several conferences on the subject (38, 40, 98, 163; see also Section 2.6.3), there are many uncertainties concerning exactly how massive stars evolve. Weaver et al. (187) calculate main sequence lifetimes for $15-M_{\odot}$ and $25-M_{\odot}$ stars that are about 2×10^6 yr longer than those indicated by curve 4. Finally, supernova explosions will occasionally occur in OB associations over a period of several $\times 10^7$ yr; such explosions, taken together with intense mass loss and continuing star formation, should further complicate H II region evolution.

2. BASIC EQUATIONS

We formulate here a system of basic equations valid for the density and temperature range expected in H II regions. Implicit in this formulation are a number of simplifying assumptions that we do not justify in detail. For example, the velocity distributions of electrons, ions, and neutral constituents of the gas are assumed to be Maxwellian at a single characteristic temperature. Any unthermalized component is treated as a small perturbation. Ions and atoms are assumed to be in the ground state. The

validity of many of these assumptions is discussed in several monographs on the subject (4, 127, 156). In addition, molecules are not considered here explicitly; thus, some modifications and additions to these basic equations are necessary in order to treat the interaction of H II regions with molecular regions in detail.

Depending on what one hopes to learn from solving this coupled system of equations [(magneto-)hydrodynamics, radiation transfer, energy conservation, and microphysical processes (such as ionization, recombination, charge exchange, thermalization of fast electrons, and molecular or atomic b-b, b-f, and f-f transitions)], varying degrees of complexity can be considered. Often one merely wishes to determine global parameters of evolution, such as the mass of ionized gas or expansion velocities as a function of time. The simplified microphysics considered is justified because the pressure structure—which mainly drives the evolution—depends primarily on the ionization structures of hydrogen and (to a lesser degree) helium. According to Rubin (140), the average electron temperature $\langle T_e \rangle$ in a photoionized nebula depends sensitively on the metal abundance (7000-K difference is possible from a factor of 10 change in abundance) and to a lesser degree on density (2900-K difference can result by changing the density from 100 to 10^5 cm^{-3}) and stellar effective temperature (1300-K difference by changing T_{eff} from 33,000 K to 45,000 K). This is consistent with results of similar studies (48, 79, 158). A range of 6000 K is observed in H II regions at varying distances from the galactic center [e.g. Shaver et al. (146)]. Thus, realistic temperatures in evolving H II regions, where accuracy to only several 10^2 K is required, can be calculated by relatively simple means (e.g. by considering only a few cooling lines). In the following we outline some of the most common simplifying assumptions and approximations.

2.1 *Magnetohydrodynamics*

The gas dynamical equations (mass conservation, motion; cf. 86) can be put into the forms

$$0 = \partial \rho / \partial t + (\mathbf{u}_{\text{rel}} \cdot \nabla) \rho + \rho \nabla \cdot \mathbf{u}, \quad 1.$$

$$0 = \partial \mathbf{u} / \partial t + (\mathbf{u}_{\text{rel}} \cdot \nabla) \mathbf{u} + 1/\rho \nabla P - \sum_i \mathbf{g}_i, \quad 2.$$

where $\mathbf{u}_{\text{rel}} = \mathbf{u} - \mathbf{u}_{\text{ref}}$ is the difference between the velocities of the gas (\mathbf{u}) and of the reference frame (\mathbf{u}_{ref}). When the reference frame moves with the gas ($\mathbf{u} = \mathbf{u}_{\text{ref}}$), one speaks of a “Lagrangian” formulation; on the other hand, when $\mathbf{u}_{\text{ref}} = 0$, the equations are said to be in a “Eulerian” formulation.

Typical acceleration terms \mathbf{g}_i to be considered in interstellar space are the radiative, gravitational, and magnetic accelerations:

$$\mathbf{g}_{\text{rad}} = \int_0^\infty dv [\kappa_v^{\text{abs}} + (1 - \langle \cos \theta \rangle) \kappa_v^{\text{sca}}] \mathbf{F}_v / c, \quad 3.$$

$$\mathbf{g}_{\text{grav}} = -\nabla\Phi, \quad 4.$$

$$\mathbf{g}_{\text{mag}} = -\frac{1}{\pi\rho} \quad 5.$$

where \mathbf{F}_v is the radiative energy flux in the frequency interval $[v, v + dv]$, and κ_v^{abs} , κ_v^{sca} are the corresponding absorption and scattering coefficients, respectively. Typical absorption processes in H II regions are photoionization and absorption by dust. Often, b-b line absorption followed by spontaneous emission can be treated as a scattering process. For isotropic scattering the mean cosine of the scattering angle ($\langle \cos \theta \rangle$) vanishes, and the extinction coefficient $\kappa_v^{\text{ext}} = \kappa_v^{\text{abs}} + \kappa_v^{\text{sca}}$ can be used in Equation 3.

The gravitational potential Φ is obtained by solving Poisson's equation: $0 = \nabla^2\Phi - 4\pi G\rho$. Often this equation can be integrated directly. For example, the solution of Equation 4 for a spherically symmetric mass distribution with mass M_r (including the mass of stars) inside radius r is given by $\mathbf{g}_{\text{grav}} = -GM_r\hat{\mathbf{r}}/r^2$, where $\hat{\mathbf{r}}$ is a unit vector in the radial direction.

The magnetic acceleration term given in Equation 5 must be supplemented by equations for the magnetic field \mathbf{B} [for example,

$$0 = \nabla \cdot \mathbf{B} \quad \text{and} \quad \partial\mathbf{B}/\partial t = \nabla \times (\mathbf{u} \times \mathbf{B}),$$

where dissipative terms have been omitted (flux-freezing approximation)]. The validity of the flux-freezing condition for partially ionized gas is discussed by Draine (41), who calculates the structure of 10 km s^{-1} magnetic shocks in a multicomponent medium in which neutral/ion slippage is considered. If $|\mathbf{B}|$ is sufficiently large, J-type shocks with magnetic precursors can exist with no discontinuities of hydrodynamic variables and with electron/ion versus neutral slippage of the order of the shock velocity.

Heiles et al. (67) derive magnetic field strengths in three H II regions from Faraday rotation measurements. For two of these (S232, S264), magnetic pressure $B^2/8\pi$ was insignificant. For S119 (the brightest part of a thick ionized shell of 23 pc diameter surrounding the O8 star 68 Cyg), a lower limit of 0.18 was obtained for the ratio of magnetic to gas pressures. This implies an even higher magnetic to gas pressure ratio at times preceding the ionization.

Multicomponent flow can be considered by including Equations 1 and 2 with frictional coupling acceleration terms \mathbf{g}_{fric} for each component

(e.g. 142, 194, 201). Alternatively, the relative motions of the various components can be treated as diffusion effects (53, 54).

Many numerical methods for solving the hydrodynamic equations incorporate an acceleration term due to artificial viscosity (\mathbf{g}_{visc}) in order to treat shock-front discontinuities. The interested reader is referred to Tscharnuter & Winkler (182) for a viable procedure for using artificial viscosity and for more detailed discussion. It should be noted that the von Neumann-Richtmyer artificial viscosity technique (cf. 136) formulated for plane-parallel geometry is inappropriate for curvilinear coordinate systems.

Finally, the solutions of the hydrodynamic equations require that the radiative flux \mathbf{F}_ν and the absorption and scattering coefficients κ_ν^{abs} , κ_ν^{sc} be known in each part of the nebula. For this purpose, equations describing the transfer of radiative energy and the state of the gas must be formulated.

2.2 Radiation Transfer

The radiation intensity $I_\nu(\mathbf{x}, \hat{\mathbf{s}}, t)$ is defined as the radiative energy flux at a point in space \mathbf{x} , where t is the time, $\hat{\mathbf{s}}$ the direction within a solid angle $d\Omega$, and $[\nu, \nu + d\nu]$ the frequency interval. It is proportional to the density of photons in phase space (cf. 116). The equation of radiation transfer (time dependent but nonrelativistic; cf. 114) can be written as

$$\frac{1}{c} \frac{\partial I}{\partial t} + (\hat{\mathbf{s}} \cdot \nabla) I = -\kappa^{\text{ext}}(I - S), \tag{6}$$

where S is the source function. Frequency subscripts are implied. The time-independent form can be obtained by allowing the speed of light c to approach infinity.

Often one considers the associated angle moment equations, where

$$J = 1/4\pi \int_{4\pi} d\Omega I,$$

$$H_i = 1/4\pi \int_{4\pi} d\Omega \cdot (\hat{\mathbf{s}})_i,$$

$$K_{ij} = 1/4\pi \int_{4\pi} d\Omega I \cdot (\hat{\mathbf{s}})_i (\hat{\mathbf{s}})_j,$$

are the moments of the radiation intensity in an orthogonal coordinate system with direction cosines $(\hat{\mathbf{s}})_i$. The zeroth moment J is related to the energy density $u = 4\pi J/c$, the first moments H_i to the radiative flux $\mathbf{F} = 4\pi \mathbf{H}$, and the second moments K_{ij} to the radiation pressure tensor.

The generalized Eddington tensor $\mathbf{f} = \mathbf{K}/J$ is often used instead of \mathbf{K} . Note that $f_{ij} = f_{ji}$ and $\text{Tr}(\mathbf{f}) = 1$, so that \mathbf{f} has in general five independent components.

The zeroth and first moment equations can be written as

$$(1/c)\partial J/\partial t + \nabla \cdot \mathbf{H} = -\kappa^{\text{abs}}J + \varepsilon, \tag{7}$$

$$(1/c)\partial \mathbf{H}/\partial t + \nabla \cdot (\mathbf{K}) = -\kappa^{\text{ext}}\mathbf{H}, \tag{8}$$

where we have implicitly assumed an isotropic source function $S = (e + \kappa^{\text{sca}}J)/\kappa^{\text{ext}}$ valid for isotropic scattering and isotropic emissivity ε of the gas. When we consider line radiation in a moving medium, κ_v^{abs} , κ_v^{ext} , and ε_v are nonisotropic and the right-hand sides of Equations 7 and 8 must be modified accordingly (cf. 114).

In spherical symmetry, H has only one nonzero component ($H = H_r$) and \mathbf{f} only one independent component ($f = f_{rr}$). Therefore,

$$\nabla \cdot \mathbf{H} = \frac{1}{r^2} \frac{\partial}{\partial r} (r^2 H) \qquad \frac{\partial}{\partial t} \qquad J$$

If, furthermore, the only source of radiation is a centrally located point source, then $f = 1$ and $\varepsilon = 0$. Equations 7 and 8 can then be simplified as follows:

$$\frac{1}{c} \frac{\partial J}{\partial t} + \frac{1}{r^2} \frac{\partial}{\partial r} (r^2 H) = -\kappa^{\text{abs}}J, \tag{9}$$

$$\frac{1}{c} \frac{\partial H}{\partial t} + \frac{1}{r^2} \frac{\partial}{\partial r} (r^2 J) = -\kappa^{\text{ext}}H. \tag{10}$$

Finally, if $\kappa^{\text{sca}} = 0$, then $J = H$ and Equations 9 and 10 are identical:

$$\frac{1}{c} \frac{\partial J}{\partial t} + \frac{1}{r^2} \frac{\partial}{\partial r} (r^2 J) = -\kappa^{\text{abs}}J. \tag{11}$$

This is the usual approximation applied to the ionizing radiation field in H II regions, which was used by Strömgren (162) in its time-independent form. Equation 11 is also valid in a nonspherically symmetric geometry, provided the same assumptions hold ($\varepsilon = 0$, $\kappa^{\text{sca}} = 0$, $f_{rr} = 1$, $f_{ij} = 0$ in a spherical polar coordinate system centered at the source). In this case κ^{abs} is a function of position (r ,) solved by integrating radially outward for each polar direction (“radial sector” approximation). If either $\kappa^{\text{sca}} \neq 0$, $\varepsilon \neq 0$, or $f_{ij} \neq \text{constant}$, then one must resort to the more general moment equations (Equations 7 and 8) using a procedure for finding f_{ij} . For spherical symmetry, efficient

numerical methods for finding f exist [cf. review by Mihalas (115); see also Yorke (196)]. If the radiation field is assumed to be isotropic or half-isotropic (either no photons moving inward or no photons moving outward), then $\mathbf{K} = (1/3)J\mathbf{I}$ and Equation 8 can be simplified in a straightforward manner (Eddington approximation):

$$\frac{1}{c} \frac{\partial \mathbf{H}}{\partial t} + \frac{1}{3} \nabla J = -\kappa^{\text{ext}} \mathbf{H}. \tag{12}$$

Thus, for the time-independent case, we have

$$\nabla \cdot \left(\frac{1}{3\kappa^{\text{ext}}} \nabla J \right) = \kappa^{\text{abs}} J - \varepsilon. \tag{13}$$

2.3 Ionization and Recombination

We denote an element with atomic number β in the r th ionization state by (β, r) and its relative abundance by x_β^r , normalized so that $\sum_{r=0}^\beta x_\beta^r = 1$. The electron density is therefore given by $n_e = n \sum_{\beta=1} \zeta_\beta \sum_{r=1}^\beta x_\beta^r \cdot r$, where ζ_β is the relative particle abundance of the element β , normalized so that $\sum_\beta \zeta_\beta = 1$. Here $n = \rho/\mu_0 m_0$ is the number density of nuclei, and $\mu_0 = \sum_\beta A_\beta \zeta_\beta$ is the mean mass per nucleus, where A_β is the mean atomic weight in amu (m_0) of a neutral atom β . For cosmic abundances, we find $\mu_0 \simeq 1.32$ [cf. Allen (3)].

Some of the principal mechanisms determining the time rate of change of x_β^r are listed below. For a description of modern atomic data banks, the interested reader is referred to the review by Zeippen (204). Otherwise, we list a few references for each type of process.

1. Photoionization (111, 124):

$$(X_\beta^r)_1 = \int_{\chi_\beta^r/h}^\infty dv (\sigma_\beta^r)_v \cdot 4\pi J_v/hv, \tag{14}$$

where $(\sigma_\beta^r)_v$ is the photoionization cross section of an ion (β, r) and χ_β^r is its ionization threshold energy. Note that

$$(\kappa_{\text{photoion}})_v^{\text{abs}} = n \sum_{\beta,r} \zeta_\beta x_\beta^r (\sigma_\beta^r)_v.$$

2. Recombination (124–126, 149, 161):

$$(X_\beta^r)_2 = n_e \sum_k \alpha_{\beta,k}^r \tag{15}$$

where $\alpha_{\beta,k}^r$ is the partial recombination coefficient of an ion (β, r) via process k .

3. Collisional ionization by thermal electrons (5, 6, 149):

$$(X_{\beta}^r)_3 = n_e C_{\beta}^r, \quad 16.$$

where C_{β}^r is the collisional ionization coefficient.

4. Charge exchange with other ions (γ, s) (6, 108):

$$(X_{\beta}^r)_4^{\pm} = n \sum_{\gamma, s} \zeta_{\gamma} x_{\gamma}^s (D_{\beta, \gamma}^{s, r})^{\pm}, \quad 17.$$

where $(D_{\beta, \gamma}^{s, r})^+ = (D_{\gamma, \beta}^{r, s})^-$ is the charge exchange coefficient when (β, r) loses and (γ, s) gains an electron.

5. Secondary (collisional) ionization by nonthermal electrons produced by photoionization with hard photons:

$$(X_{\beta}^r)_5 = \sum_{\gamma, s} \zeta_{\gamma} x_{\gamma}^s \int_{(\chi_{\beta}^r + \chi_{\gamma}^s)/h}^{\infty} dv E_{\beta}^r (h\nu - \chi_{\gamma}^s) (\sigma_{\gamma}^s)_v 4\pi J_{\nu} / h\nu. \quad 18.$$

The mean number of secondary ionizations $E_{\beta}^r(e)$ per nonthermal electron of energy e must take into account partial thermalization and competition with other "destruction" mechanisms (excitation of low-lying levels and ionization of other species). Thus E_{β}^r depends on the local ionization structure, density, and temperature of the gas.

6. Ionization by cosmic rays (both primary and secondary ionizations):

$$(X_{\beta}^r)_6 = \Psi_{\beta}^r + \sum_{\gamma, s} \zeta_{\gamma} x_{\gamma}^s \Psi_{\gamma}^s E_{\beta}^r (e_{\gamma}^s), \quad 19.$$

where Ψ_{β}^r is the primary ionization rate of an ion (β, r) by cosmic rays, and e_{β}^r is the average energy of the ejected electron.

7. Ionization by recombination photons "on the spot": Let us denote $\phi_{\gamma, k}^s(\nu)$ the frequency distribution of photons emitted by each recombination of an ion (γ, s) via process k (including subsequent radiative transitions to the ground state). In many cases $\phi_{\gamma, k}^s(\nu)$ can be treated as a sum of Kronecker delta functions, weighted when necessary by appropriate branching ratios. The contribution from two-photon transitions and from the thermal velocity spread of recombining electrons is continuous. For each type of recombination process, $\phi_{\gamma, k}^s(\nu)$ obeys the relation $\int dv [\phi_{\gamma, k}^s(\nu) h\nu] \geq \chi_{\gamma}^s$. These photons are a source of emissivity of the gas:

$$(\epsilon_{\text{rec}})_{\nu} = n n_e \sum_{\gamma, s, k} \zeta_{\gamma} x_{\gamma}^s x_{\gamma, k}^s \phi_{\gamma, k}^s(\nu) h\nu / 4\pi. \quad 20.$$

Because of the linearity of the radiation transport equations, this contribution to J_{ν} can be treated separately. Use of the time-independent Eddington approximation (Equation 13) is justifiably accurate for many

purposes. Usually, however,

$$(\mathbf{J}_{\text{rec}})_v = (\epsilon_{\text{rec}})_v / \kappa_v^{\text{abs}} \quad 21.$$

is substituted directly into Equations 14 and 18 (“on-the-spot” approximation), a procedure that is valid when $1/\kappa_v^{\text{abs}}$ is small compared with the length scales of interest.

Using these definitions, we can write the time rate of change of x_β^r as

$$\begin{aligned} \frac{\partial x_\beta^r}{\partial t} + (\mathbf{u}_{\text{rel}} \cdot \nabla) x_\beta^r \\ = x_\beta^{r-1} [(X_\beta^{r-1})_1 + (X_\beta^{r-1})_3 + (X_\beta^{r-1})_4^+ + (X_\beta^{r-1})_5 + (X_\beta^{r-1})_6] \\ - x_\beta^r [(X_\beta^r)_1 + (X_\beta^r)_2 + (X_\beta^r)_3 + (X_\beta^r)_4^+ + (X_\beta^r)_4^- + (X_\beta^r)_5 + (X_\beta^r)_6] \\ + x_\beta^{r+1} [(X_\beta^{r+1})_2 + (X_\beta^{r+1})_4^-], \end{aligned} \quad 22.$$

where it is implicitly assumed that

$$x_\beta^{r-1} = x_\beta^{r+1} = (X_\beta^0)_2 = (X_\beta^0)_4^- = (X_\beta^0)_4^+ = (X_\beta^0)_{1,3,5,6} = 0.$$

For each element β , there are β such equations, one of which may be replaced by the normalization condition. Chemical reactions with the ion (β, r) may also be important in molecular regions bounding H II regions where shocks are present (117, 118, 186), but their effects have generally been ignored in hydrodynamical evolution calculations of H II regions. The main reaction types are discussed by Watson (185). Prasad & Huntress (132, 133) list 1423 reactions for 137 species, but only about 25% of their reaction rates are based on laboratory measurements; the remainder can be expected to be accurate to perhaps an order of magnitude. However, some important photo-processes are missing from their scheme (e.g. photodissociation of H_2), which restricts its application in zones close to H II regions.

2.4 Thermal Energy Balance

The conservation of thermal energy can be expressed as

$$0 = \frac{\partial E}{\partial t} + (\mathbf{u}_{\text{rel}} \cdot \nabla) E + \frac{P}{\rho} (\nabla \cdot \mathbf{u}) + \frac{\Lambda - \Gamma}{\rho}, \quad 23.$$

where $E = (3/2)kT(n + n_e)/\rho$ is the thermal energy of the gas per unit mass, and Λ and Γ are the rates of thermal energy losses and gains per unit volume not included in the (de-)compressional work term $P/\rho(\nabla \cdot \mathbf{u})$. Care must be exercised when determining which microphysical processes modify

E via Λ and Γ . When, for example, an ion/electron pair radiatively recombines, E is modified indirectly as a result of the change in n_e/ρ . The contribution to Λ is only about 0.3 $[(3/2)kT]$ per recombination, because slow electrons are generally favored in the recombination process. Using the symbols defined above, we may write

$$\Lambda_{\text{rec}} = nn_e \sum_{\gamma,s,k} \zeta_{\gamma} x_{\gamma}^s \alpha_{\gamma,k}^s \cdot \left\{ \int dv [\phi_{\gamma,k}^s(v) hv] - \chi_{\gamma}^s \right\}. \quad 24.$$

Collisional ionization by thermal electrons will also contribute to Λ :

$$\Lambda_{\text{coll}} = n_e n \sum_{\beta,r} \zeta_{\beta} x_{\beta}^r \chi_{\beta}^r C_{\beta}^r. \quad 25.$$

Collisions of atoms and molecules with dust grains could contribute significantly to the thermal balance of neutral gas, especially at high gas densities, when collisional deexcitation and optical depth effects may become important. Such collisions have little effect on the grain temperature. The temperature $T_{\text{dust}}^{(i)}$ of a grain (i) of given composition and size is given by the thermal equilibrium condition

$$0 = \int dv (\kappa_{\text{dust}}^{(i)})_v^{\text{abs}} [J_v - B_v(T_{\text{dust}}^{(i)})],$$

where B_v is the Planck function. When the grains have no net motion with respect to the gas, we have

$$(\Lambda - \Gamma)_{\text{dust}} = n \sum_{\beta} \zeta_{\beta} v_{\text{th}}^{\beta} \sum_i \pi a_i^2 n_{\text{dust}}^{(i)} \eta_{\beta}^{(i)} k(T - T_{\text{dust}}^{(i)}),$$

where $n_{\text{dust}}^{(i)}$ is the particle density of grain type (i), πa_i^2 the grain's geometrical cross section, $\eta_{\beta}^{(i)}$ the efficiency of energy transfer usually assumed to be of order unity, and v_{th}^{β} the thermal velocity of the neutral constituent β of the gas. Typically, only hydrogen need be considered. When grains move with respect to the gas or they interact principally with charged particles, the situation is much more complex. Depending on the ratio of the density of energetic photons that remove electrons from the grain surface (photoelectric effect) and the electron density, grains can be either positively or negatively charged (e.g. 54, 94, 119). This affects the thermal and hydrodynamical coupling between dust grains and gas. Partly as a result of the grain's charge, gas/grain collisions are unimportant for the thermal balance of fully ionized gas.

The heating of H II regions by photo-ejected electrons from grains by stellar continuum and recombination $\text{L}\alpha$ photons has been considered by Maciel & Pottasch (95), who find some influence on the thermal structure.

By far the most effective mechanism for removing thermal energy from the ionized gas is line radiation following collisional excitation by thermal

electrons of low-lying levels in atoms, molecules, and ions. Except in special cases (i.e. maser emission, optically thick lines, or continuum), it suffices to consider collisional excitation, deexcitation, and spontaneous emission only. For many ions, only one excited level need be considered, and often collisional deexcitation is negligible. Thus, cooling rates can often be written in a form comparable to Equation 25. Detailed discussions of cooling processes, including free-free transitions, can be found in several current monographs (4, 127, 156). Updated atomic data have been compiled by Mendoza (111). This compilation is included in Aller's monograph (4) as an appendix.

The partial thermalization of energetic electrons produced by (a) photoionization and (b) cosmic-ray ionization will contribute to thermal energy gains in the gas :

$$\Gamma_1 = n \sum_{\beta,r} \zeta_{\beta} x_{\beta}^r \int_{\chi_{\beta}^r/h}^{\infty} dv (\sigma_{\beta}^r)_v 4\pi J_v h\nu \cdot [h\nu - \chi_{\beta}^r - \Delta E(h\nu - \chi_{\beta}^r)], \quad 26.$$

$$\Gamma_2 = n \sum_{\beta,r} \zeta_{\beta} x_{\beta}^r \Psi_{\beta}^r \cdot [e_{\beta}^r - \Delta E(e_{\beta}^r)], \quad 27.$$

where $\Delta E(e)$ is the energy that nonthermal electrons of energy e lose via secondary ionizations $[\sum_{\gamma,s} \zeta_{\gamma} x_{\gamma}^s \chi_{\gamma}^s E_{\gamma}^s(e)]$ and via collisional excitation of low-lying levels that subsequently spontaneously emit photons. When an on-the-spot approximation is used, the appropriate contribution to J_v (given in Equations 20 and 21) can be substituted directly into Equation 26. Heating by artificial viscosity Γ_{visc} consistent with \mathbf{g}_{visc} should also be included (cf. 182).

2.5 Boundary Conditions and Initial Values

The coupled system of partial differential equations introduced in the preceding sections defines an initial-value problem requiring boundary conditions. Generally speaking, whenever information is transmitted across a boundary into the region under consideration (either by gravitation, advection, radiation, or magnetic fields), appropriate boundary conditions must be tailored to the particular problem at hand.

Consider, for example, the nonmagnetic system of equations (Equations 1, 2, 11, 22, 23) that describe the time rate of change of the dependent variables ρ , \mathbf{u} , J_v , x_{β}^r , and E , from which T and P can be calculated. At the inner boundary in a spherically symmetric geometry, one should specify values for M_r , J_v , and fluxes ρu , $\rho u x_{\beta}^r$, ρu^2 , $\rho u E$ when $u > 0$, as appropriate for a given source of stellar wind and stellar radiation. The outer boundary conditions should specify the appropriate matter, momentum, and thermal

energy fluxes when $u < 0$. If outside sources of ionizing radiation are included (for example, in the case of a globule immersed in an H II region), Equation 11 (which implies an Eddington factor of $f = 1$) is unrealistic and should be replaced by the more general moment equations (Equations 7 and 8, 9 and 12 or 13). Boundary conditions for J_v and (if necessary) \mathbf{H} , must then be given.

In the full time-dependent formulation of the numerical problem, initial values for each of the dependent variables must be specified. This requirement can be relaxed when steady-state solutions are sought, i.e. $\partial h/\partial t = 0$ for all dependent variables h . Static model nebula are calculated assuming $\partial h/\partial t = 0$ and $u = 0$; this eliminates the need to solve the hydrodynamic equations and simplifies somewhat the line transfer problem. In this case, the microphysics can be considered in much greater detail, which is useful for checking the validity of some simplifying assumptions.

2.6 *State of the Art of Numerical Evolution Calculations of H II Regions*

From the above discussion it should be clear that time-dependent calculations of the evolution of H II regions depend on detailed knowledge of (a) microphysics, (b) boundary conditions, and (c) initial values for the distributions of dependent variables as outlined above. Recent theoretical advances have come from more realistic treatment of each of these factors, together with improved numerical methods and larger, faster computers. However, there is still much room for improvement. In Table 2 the present status of evolution calculations is summarized.

2.6.1 MICROPHYSICS Because of their importance for the interpretation of a number of astrophysical objects, ranging from the narrow-line region (NLR) and broad-line region (BLR) clouds of active galactic nuclei to compact H II regions and planetary nebulae, static model calculations of H II regions have attained a high degree of sophistication regarding the detailed microphysics considered (e.g. 2, 48, 49, 78, 79, 140, 158, and references therein).

Multicomponent hydrodynamics has been considered in evolving ionized regions (53, 54, 142, 194, 195). Gail & Sedlmayr (54) find no significant separation of gaseous components but significant separation of dust and gas in the I-front and neutral boundary zones (see also 194, 195, 201). Magnetic fields have not yet been considered in multidimensional hydrodynamical evolution models, although their possible importance and some consequences can already be surmised from one-dimensional studies with simplifying assumptions [e.g. those by Lasker (92) and Pascoli (130) for planetary nebulae].

2.6.2 BOUNDARY CONDITIONS The boundary conditions and initial values for the dependent variables actually define the problem considered. When the heavy-element ionization structure is desired, for instance, for line profile calculations in dynamically evolving H II regions, detailed knowledge of the spectral distribution of the stellar flux in aging stars is necessary. The calculated LTE, line-blanketed atmospheres of, e.g., Kurucz (81) and the NLTE, unblanketed atmospheres of Mihalas (113) can be used, as can corresponding atmospheres calculated using their computer codes [e.g. Borsenberger & Stasinska (24)] or other available codes [see Baschek & Scholz (12) for a description of the numerical/mathematical problem]. Line blanketing, a major UV opacity source, is probably even more effective than indicated by Kurucz's models, because the opacity distribution functions used are incomplete in lines of higher metal ions [cf. Baschek et al. (11)]. Self-consistent NLTE, blanketed, and (in particular) nonstatic atmospheres are unfortunately not available and cannot be expected in the near future.

There is also considerable uncertainty regarding the fate of evolving O and B stars during late main sequence burning phases. Recent theoretical work [reviewed by Maeder (96, 97) and Chiosi & Maeder (30)] has shown that depending on initial mass and mass-loss rates, the more massive stars may go through very different evolutionary sequences. Competing effects (such as classical envelope expansion with core contraction; helium core growth; homogenization of the envelope by a large, fully convective zone; and large luminosity-to-mass ratios, which favor envelope expansion) determine whether a star evolves blueward or redward from the ZAMS. The poorly known mass-loss rate during these late main sequence phases thus not only is a critical parameter for the interaction of stellar winds with H II regions, but also is of crucial importance for something as basic as the flux of Lyman continuum (Lyc) photons as a function of time. Although incomplete knowledge of internal mixing processes [e.g. overshooting and semiconvection; see discussions in (28–30, 36, 87)] and of binary star evolution [deLoore (37)] hampers even further any quantitative predictions of the time evolution of the stellar UV flux, it seems likely that very massive stars may spend a substantial percentage of their nuclear-burning lifetimes blueward of the ZAMS. This fact has encouraged Terlevich & Melnik (173) to suggest that the central ionizing source of Seyfert 2 and Liner nuclei could be a 3×10^6 -yr-old OB cluster resulting from a previous burst of star formation. Using (unpublished) Maeder evolutionary tracks, Kurucz (81) atmospheres redward of the ZAMS, and helium atmospheres of Wesemael (189) blueward in accordance with the calculated chemical composition of the outer stellar layers, Terlevich & Melnik (173) find that such a cluster should contain a substantial number

Table 2 Present state of the art of numerical hydrodynamic and static nebulae calculations, summarizing what has been considered and neglected in published work to date^a

Physics considered	Symmetry assumed	One-dimensional spherical, slab	Two-dimensional cylindrical	Static ionization models
Hydrodynamics		Implicit, explicit	Explicit	—
Spatial resolution		Good	I-front unresolved	Good
Gravity		+	+	—
Magnetic fields		○	—	—
Radiative acceleration :				
(a) dust		+		
(b) b-b, b-f transitions, e ⁻ scattering		○	—	—
Multicomponent flow, diffusion effects		+	○	—
Atomic processes :		H He C, N, O, ...	H He C, N, O, ...	H, He, C, N, O, ...
(a) heating/cooling		+ + ○	○ — ○	+
(b) ionization/recombination		+ + —	○ — —	+

Ionizing radiation transport :			
(a) Continuum from star	+	+	+
(b) diffuse continuum	○	○	+
(c) lines	On the spot	On the spot	○
Nonionizing radiation transport :			
(a) continuum	+	○	+
(b) recombination photons, cooling lines	○	—	○
Molecular chemistry	○	—	○
Evolution of ionizing sources	+	+	—
Stellar winds	+	—	○
Nonconstant initial density	+	+	○
Protostellar evolution prior to ionization	○	—	—

*Symbols as follows: + considered, numerical method (in principle) accurate—improvements in microphysics still possible; ○ considered, numerical method approximate or crude; — not considered. No single investigation has treated all effects listed with + or ○, although static nebulae codes come closest to this capability.

of extremely hot ($T_{\text{eff}} > 10^5$ K), massive stars (“warmers”), and that the predicted overall UV spectrum resembles the power-law spectrum assumed by Ferland & Netzer (49) to explain Seyfert 2 and Liner line ratios by metal-rich massive H II regions.

Using both published evolutionary tracks of 25 representative single stars (without mass loss, with conventional convective mixing, but with no overshooting) and Kurucz et al. (82) model atmospheres, Beltrametti et al. (15) calculate the time rate of change of Lyc photons of OB associations with varying initial mass functions. The evolution of an H II region surrounding such an OB cluster is discussed in Section 3.

The existence of stellar winds can have important consequences regarding the structure and evolution of H II regions—to the point that either the H II region is squelched out of existence (see Section 3.2.1) or else one begins to speak of entirely different objects. Such objects include bipolar (or biconical) nebulae, planetary nebulae, ring nebulae, stellar wind bubbles, etc, some of which are subjects of recent reviews in this series (30, 44, 77, 85).

2.6.3 INITIAL VALUES Relaxation of the “constant-density” initial condition has allowed progress to be made in matching morphological shapes and overall velocity patterns obtained in numerical hydrodynamical evolution calculations of H II regions to their observed counterparts (champagne model, blister model; see Section 3). In addition, the realization that the formation of compact and ultracompact H II regions is intimately related to the formation and evolution of massive stars, and in particular to details of the evolution of the protostellar envelopes prior to ionization, has sparked interest in these early evolutionary phases.

2.6.4 NUMERICAL METHODS OF SOLUTION The most popular technique of numerical solution of the coupled partial differential equations described above has been the use of finite differences. At least some of these equations (i.e. Equations 22 and 23) should be formulated with backward or centered time differences and solved iteratively (implicit schemes). The hydrodynamical equations can be formulated and solved using forward time differences (explicit schemes) as long as the Courant-Friedrichs-Levy condition $\Delta t < f\Delta l/(u^2 + v_{\text{th}}^2 + v_a^2)^{1/2}$ does not impose too stringent a requirement on the size of the time step Δt with respect to the evolutionary time under consideration. (Here Δl , u , v_{th} , and v_a are the local grid spacing, gas velocity, isothermal sound speed, and Alfvén velocity, respectively). When high-velocity stellar winds are considered, implicit hydrodynamic schemes may be required. Fully implicit two-dimensional hydrodynamic codes

designed to follow the evolution of H II regions do not exist at present. Use of second order and higher difference schemes in one-dimensional and two-dimensional codes in order to improve the spatial resolution of fronts and contact discontinuities is becoming more common.

3. THE FORMATION AND EVOLUTION OF H II REGIONS

3.1 *The “Classical” Model for the Evolution of S-Type H II Regions*

By solving numerically the equation of transport for hydrogen-ionizing photons together with the condition for ionization/recombination equilibrium in a constant-density medium, Strömgren (162) showed that spheres of almost fully ionized gas should exist around hot O stars with a rather sharp transition to the outlying, almost fully neutral gas. Strömgren furthermore pointed out that these photons have more energy than necessary to merely ionize hydrogen, and thus they should be important for heating the gas. As shown later by Spitzer & Savedoff (157), this energy excess causes an H II region to heat up to a temperature of approximately 10^4 K, about a factor of 100 higher than the temperature of the ambient neutral gas. Thus, ionized nebulae were expected to expand as a result of the pressure difference between ionized and neutral material.

In the following years, the “classical” theory for the evolution of H II regions was developed by many investigators [see the review by Mathews & O’Dell (106) for a list of references up to 1969]. Kahn (76), Axford (7), and Goldsworthy (59) developed the basic formalism and nomenclature of steady-state I-front physics, and the formation of shock fronts preceding I-fronts under certain circumstances was predicted. The first computer studies of H II region evolution began in the 1960s (e.g. 68, 91, 105; see also 174), and these confirmed in detail what then had already been surmised from analytic studies. Analytic and numerical computational studies continued with improved and more detailed microphysics, and by the end of the 1970s the “classical” evolutionary picture of H II regions had emerged as the standard for which to compare the relative importance of competing effects and any new processes being considered and/or to test new numerical methods (53, 54, 60, 63, 99–103, 164).

The problem considered for the classical evolution is the following. A hot early-type star begins to emit ionizing photons in a uniform neutral medium of infinite extent that is at rest. After several million years, the ionizing flux decreases. The evolution of the ambient medium is divided into three phases: the formation phase, the expansion phase, and the recombination phase. We consider each briefly here. A discussion of the

approximations that can be applied and the scaling laws appropriate for the first two phases is given by Goldsworthy (60), who generalizes the numerical solutions to a wide variety of initial densities and ionizing fluxes.

3.1.1 THE FORMATION PHASE When the ionizing point source switches on, an I-front sweeps through the gas at supersonic velocity

$$r_i = \min \left\{ c, \frac{1}{4\pi n_H r_i^2} \left[S_u(0) - \frac{4\pi}{3} r_i^3 n_H^2 \alpha^{(2)} \right] \right\},$$

ionizing and heating it but otherwise leaving it undisturbed. Here we have amended Spitzer's (156) formula for a point source at $r = 0$ in a pure hydrogen gas to account for the finite speed of light [n_H is the particle density, $S_u(r)$ the number of ionizing photons per unit time passing through a sphere of radius r , and $\alpha^{(2)}$ the coefficient for recombinations into level 2 and higher ("on-the-spot" approximation for a dust-free hydrogen gas)]. This so-called weak R-type I-front [see, e.g., Spitzer (156) for a discussion of I-front notation] persists until its location r_i is about 2% of the Strömngren radius $r_s = [3S_u(0)/4\pi n_H^2 \alpha^{(2)}]^{1/3}$. Modifications, such as gradual turn-on of the ionizing source, competition of dust and helium for ionizing photons, non-steady-state gas dynamics, or time-dependent ionization/recombination, require a detailed numerical treatment. As r_i approaches r_s , the I-front slows and changes from weak R-type to subsonic D-type, evolving through strong-D, critical-D, and finally weak-D phases (106, 164) as a shock front forms and detaches from the I-front. This marks the beginning of the expansion phase.

3.1.2 THE EXPANSION PHASE The heated sphere of ionized gas expands against the surrounding neutral medium bounded by a weak D-type I-front and its associated shock. The global expansion lowers the density in the ionized sphere, thus lowering the recombination rate and making more photons available to ionize the gas. The mass of ionized gas therefore increases with expansion. The I-front and shock front are separated by a geometrically thin shell of neutral shocked gas. Their radii approximately follow the formula (cf. 156)

$$r_i = r_s \left(1 + 7/4 \frac{C_{II}(t - t_0)}{r_s} \right)^{4/7},$$

where C_{II} is the isothermal sound speed of the ionized gas. This formula implies a maximum gas velocity of $C_{II} \simeq 10 \text{ km s}^{-1}$, which subsequently decays to $(1/2)C_{II}$ for $r_i = 2.5r_s$, corresponding to about 5 (or 0.05) Myr

for an O5 star in a medium of density $n_{\text{H}} = 10 \text{ cm}^{-3}$ (or 10^4 cm^{-3}). In addition to the hydrodynamic calculations cited above, steady-state weak D-fronts have been calculated by Mallik (99) and Harrington (63), who paid particular attention to nonequilibrium heating/cooling and ionization/recombination. Mallik's large predicted deviations from the equilibrium temperature within the I-front were shown later by Harrington to be actually less than 10^3 K . Such deviations still can affect strongly the [O I] $\lambda 6300$ line strengths, since they originate primarily in I-front regions. Repeating Mallik's case 2, for which $T_{\text{max}} = 16,000 \text{ K}$ is given, Harrington calculates $T_{\text{max}} = 9200 \text{ K}$ and concludes that the analysis of Axford (7) and Goldsworthy (59) is adequately valid.

The expansion ends either when pressure equilibrium is attained between ionized and neutral regions ($r_i \simeq 5r_s$) or when the ionizing source moves off the main sequence, marking the beginning of the recombination phase.

3.1.3 THE RECOMBINATION PHASE The evolution of H II regions during the recombination phase depends on the details of how the ionizing flux changes with time. Manfroid (100, 102) has followed the time-dependent recombination of a diffuse nebula in which the single exciting star has moved off the main sequence. Considering more than 100 forbidden lines and ionizations of elements up to 120 eV, he finds that the forbidden lines decay more rapidly than those of hydrogen and helium, so that charge exchange reactions are particularly important for the resulting spectrum. Beltrametti et al. (15) have calculated the recombination phase for two types of ionizing sources but with less detailed microphysics. Source L1 was assumed to consist of several O stars, one of which suddenly leaves the main sequence, which causes the ionizing luminosity to decrease from $2 \times 10^{49} \text{ Lyc photons s}^{-1}$ to half that value. Source L2 was chosen to model an OB association with a continuous decrease of the Lyc flux. Considering the various cases calculated, including those described by Tenorio-Tagle et al. (171), we can make the following general remarks. The decrease in ionizing flux causes the I-front to recede, supersonically if the drop in flux is sufficiently rapid. The neutral, newly recombined gas still expands as a result of its inertia, and it is still preceded by the now momentum-driven shock front moving into the undisturbed neutral medium. During this phase the H II region has the appearance of an expanding sphere of ionized gas surrounded by a geometrically thick shell of expanding neutral gas ($u \lesssim 10 \text{ km s}^{-1}$) at about the same density. For the calculated cases with the L1 source, the I-front begins to move outward again when the Strömgren radius corresponding to the remaining flux is reached. The I-front is again of weak-D type, but it now travels through an expanding neutral medium. Eventually the two shocks merge, and

“classical” expansion continues until the next star moves off the main sequence. We defer the discussion of L2 cases until Section 3.4.

3.2 The Formation Phase—Late Stages of Star Formation

In 1979 Habing & Israel (62) extensively reviewed the research of compact H II regions and OB star formation. We assume that the reader is acquainted with this work and discuss certain theoretical aspects not considered in their review.

3.2.1 IONIZED SPHERES IN FLOWING ENVELOPES A simple procedure can be used to estimate the equilibrium size of an H II region in a $\rho \sim r^{-\alpha}$ envelope resulting from steady-state inflow or outflow (cf. 198). We consider hydrogen only, with negligible dust absorption, and assume the on-the-spot approximation for Ly α photons resulting from recombinations directly into the ground level. We use Equations 11, 14, 15, 20, 21, and 22, together with the simplifying assumptions leading to their derivation, and assume furthermore that the degree of ionization changes discontinuously from $x \simeq 1$ to $x \simeq 0$ at $r = r_i$. After algebraic manipulation, we find that

$$r_i = r_1 [1 + (3 - 2\alpha) \dot{M}_{\text{cr}}^2 / \dot{M}^2]^{1/(3 - 2\alpha)} \quad 28.$$

for $\alpha \neq 3/2$ or

$$r_i = r_1 \exp[\dot{M}_{\text{cr}}^2 / \dot{M}^2] \quad 29.$$

for $\alpha = 3/2$. Here \dot{M}_{cr} is a critical accretion (outflow) rate defined by

$$\begin{aligned} \dot{M}_{\text{cr}} &= [4\pi\mu_0^2 m_0^2 S_{\text{eff}} r_1 v_1^2 / \alpha^{(2)}]^{1/2} \\ &\simeq 6 \times 10^{-6} M_{\odot} \text{ yr}^{-1} \left(\frac{v_1}{100 \text{ km s}^{-1}} \right) \left(\frac{r_1}{10 R_{\odot}} \right)^{1/2} \left(\frac{S_{\text{eff}}}{10^{49} \text{ s}^{-1}} \right)^{1/2}, \end{aligned}$$

where v_1 is the gas velocity at the base of the ionized region at radius r_1 , and $S_{\text{eff}} = S_u(r_1) + \dot{M} / \mu_0 m_0$ is the rate of ionizing photons passing through this radius [$S_u(r_1)$], corrected by an advection term $\dot{M} / \mu_0 m_0$ (positive for outflow, negative for inflow). For a mass loss $\dot{M} = 1.7 \times 10^{-6} M_{\odot} \text{ yr}^{-1}$ ($7 \times 10^{-5} M_{\odot} \text{ yr}^{-1}$), this correction term is $\dot{M} / \mu_0 m_0 \simeq 5 \times 10^{43} \text{ s}^{-1}$ ($2 \times 10^{45} \text{ s}^{-1}$) and corresponds to the Ly α luminosity of a ZAMS B3 (B1) star, according to Panagia’s (128) table. Accretion flows can contribute significantly to the Ly α flux via accretion shocks. Such inflows will also have dusty cocoons at a radius (inner cocoon) $r_c \simeq 2 \times 10^{13} \text{ cm}$ ($L/10^3 L_{\odot}$)^{1/2} (cf. 198), which invalidates the assumption of negligible dust absorption beyond this radius. Simon et al. (150) demonstrate that photoionization of hydrogen from level 2 can be an important ionization mechanism

for very dense circumstellar envelopes, where both radio continuum and hydrogen IR line emission are optically thick. In this case, $S_u(r)$ should include the stellar Balmer continuum photon flux, which Thompson (176) has tabulated using Kurucz (81) atmospheres, updating also Panagia's (128) table for the Lyc flux. Simon et al. furthermore calculate the infrared line and radio continuum emission of such density-peaked regions ($\alpha > 0$), leaving the outer boundary r_i as a free parameter. As a result of the above-mentioned effects, the magnitude of S_{eff} for a particular source is uncertain, even when the observed bolometric luminosity allows a tentative ZAMS spectral-type identification. Previous analysis of the continuum radio emission (129, 192) and hydrogen IR lines (80, 151) considered the ionized flow to extend to infinity.

Inspection of Equations 28 and 29 shows that an E-type H II region will be able to propagate outward from an ionizing source only when the ratio \dot{M}/v_1 is sufficiently low. When the mass flow is direction dependent, these equations are still valid—in the radial sector approximation—when applied to each solid angle. Thus, it is possible for an ionization front to propagate outward in some directions and be squelched ($\dot{M} \gg \dot{M}_{\text{cr}}$) in others.

3.2.2 NUMERICAL CALCULATIONS OF COMPACT H II REGION FORMATION

The hydrodynamical and spectral evolution of a $10-M_{\odot}$ spherically symmetric protostellar cloud from initial gravitational collapse until the formation of an expanding compact H II region surrounding a $9.5-M_{\odot}$ ZAMS star has been calculated by Yorke (194, 195); these calculations include the effects of gas/dust slippage, frequency, and angle-dependent continuum radiation transfer. The evolution of several important radii is shown in Figure 2. After a little longer than one free-fall time a hydrostatic core forms at the center, containing a small fraction of the original mass. About 4.1×10^4 yr later the core contains a mass of $6.9 M_{\odot}$ and has contracted to the main sequence radius $r_* \simeq 2 \times 10^{11}$ cm. It continues to grow in mass, and at an age $t \simeq 1.5 \times 10^5$ yr the refractory (graphite and silicates) grains decouple dynamically from the gas, drift outward despite continuing gas infall, and recouple in the outer regions, which prevents further infall of material beyond $\sim 10^{16}$ cm. Inside this radius the dust-free gas approximates well a freely falling inflow with velocity $v(r) = -\sqrt{2GM/r}$ and density $\rho \sim r^{-3/2}$, and the arguments given in Section 3.2.1 apply. The rapid transition of an extremely compact H II region of radius $r_{\text{H II}} \simeq 3r_*$ to a compact H II region of radius $r_{\text{H II}} \simeq 3 \times 10^{16}$ cm is understandable in terms of decreasing \dot{M}/v at the stellar surface. The I-front crosses the radius r_{R} beyond which refractory grains are present, and the ultracompact H II region expands, preceded by a dusty cocoon. The final

model calculated in the evolutionary sequence is a compact H II region of radius $r_{\text{H II}} = 10^{17}$ cm. About 7/8 of its ionized volume is filled with refractory dust at temperature $T_{\text{R}} < 100$ K, whereas the inner parts are dust free. Hot 10^3 K dust and its associated near-IR emission are absent.

For the $50-M_{\odot}$ and $150-M_{\odot}$ protostellar clouds, which produced main sequence stars of mass $16 M_{\odot}$ and $36 M_{\odot}$, respectively [calculated by Yorke & Krügel (201)], the calculations were stopped immediately prior to H II region formation because of oscillations [of physical origin; see also Garlick (55)] that restricted the size of the time step. Still, dense

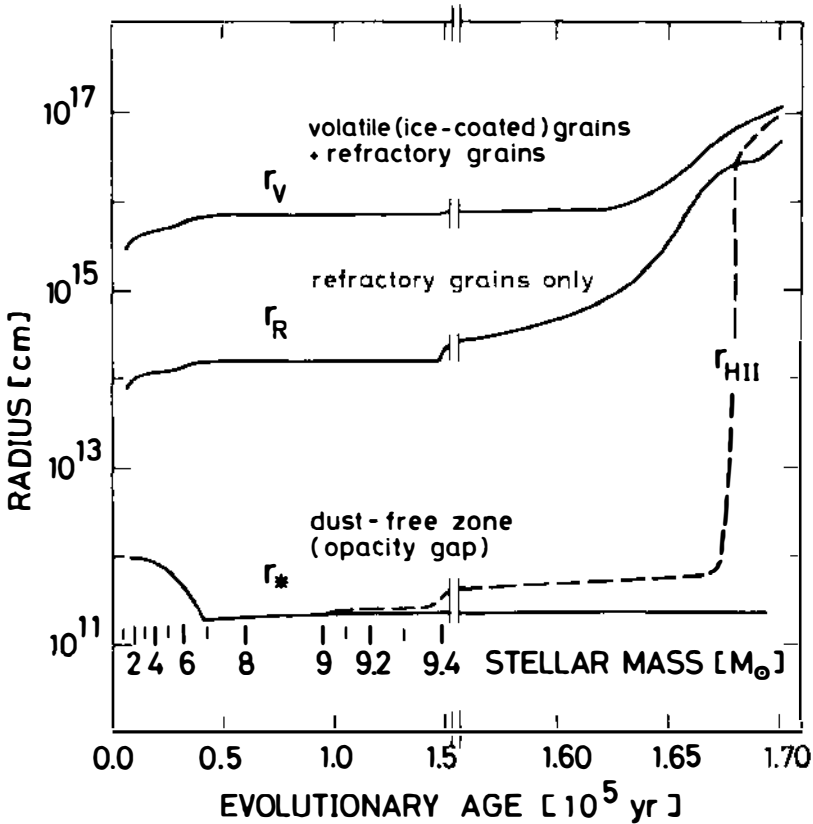


Figure 2 Time evolution of the boundaries of various zones in the protostellar envelope. Here r_* is the (proto-)stellar radius and location of the accretion shock front, $r_{\text{H II}}$ is the radius of the I-front, r_{R} is the grain destruction radius of refractory particles, and r_{v} is the radius of volatile ice mantle destruction. Note the change of scale at 1.55×10^5 yr. The mass accreted onto the central core corresponding to the evolutionary age after core formation is also given. The figure is adapted from Yorke (197).

cocoon shells at $r \sim r_v$ were formed, which (as in the $10-M_\odot$ case) halted the inflow. Compact H II regions of S-type can be expected to form interior to this outer cocoon after mass infall decreases sufficiently.

The calculations described above have the great disadvantage that rotation was not included. Two-dimensional numerical calculations of H II region formation are necessary that allow accretion onto the central source via an accretion disk and mass outflow along the symmetry axis.

3.2.3 COMPACT H II REGION FORMATION WITH ROTATION AND OUTFLOW

Even a small amount of rotation in the protostellar cloud can affect dramatically the evolution of the central source prior to the formation of a compact H II region [cf. Bodenheimer (21)]. Without angular momentum transport, a disk rather than a protostar is formed. Magnetic braking may have previously reduced the angular momentum by a factor of several orders of magnitude [cf. Mouschovias (122)], but this process is no longer effective in dense protostellar disks due to the extremely low degree of ionization. In analogy to the evolution of a $3-M_\odot$ rotating protostellar cloud calculated by Tscharnuter (181), the more massive rotating cloud can be expected to form a disk at its center, which subsequently grows in mass and size as it accretes material from the infalling envelope. Poorly understood viscous processes transport angular momentum outward and material inward within the disk, and thus the inner part of the disk evolves toward a more compact starlike condensation. As in the nonrotating case, this starlike condensation will contract toward main sequence densities and temperatures, but its evolution may be strongly influenced by the time scale of angular momentum transport. The mere existence of massive stars and the lack of observed pre-main sequence stars with $M > 5 M_\odot$ show that at least these stars have solved their angular momentum problem within the accretion time scale (curve 3 in Figure 1).

Mass outflow appears to be a general phenomenon associated with the star formation process (cf. 8, 58, 148, 152). In particular, one can expect all stars that evolve into main sequence late or early B-types to go through a phase of intense but relatively low-velocity mass loss [see discussion and models by Dyson (46)]. The Orion region is the most well-studied star formation region, and it is therefore not surprising that mass outflow and shock-induced H_2 emission were first discovered in the Kleinmann-Low (KL) region (56, 84, 206). In the controversy over whether the "disk" surrounding IRC2 near the Orion KL region is truly a disk [Kutner et al. (83)] or merely colliding clouds [Ho & Barrett (69)], the former interpretation seems more likely to be correct [Vogel et al. (184)]. This and other tentative disk identifications around luminous IR sources suggest that outflows from massive objects can occur concurrently with disks. Disks

are often invoked in theoretical models of collimated outflow [cf. (134, 135, 138, 179, 180) for recent examples and references], although there is far from a general consensus of opinion regarding either the acceleration or the collimation mechanisms [see, e.g., Draine (42) for a purely “magnetic” interpretation]. In any case, the first stage of H II region evolution may be of E-type in a collimated (bipolar) outflow when the ratio \dot{M}/v_1 is sufficiently low; the nebula may later evolve into an S-type H II region (as described in Section 3.2.2) when inflow from the protostellar envelope onto the accretion disk stops and it begins to shrink in size and importance. A fossil accretion disk with associated collimated outflow may persist, but it will no longer dominate the subsequent H II region expansion.

Dreher et al. (43) noted that the ultracompact H II regions they observed in W49N should have lifetimes of $\sim 10^5$ yr, rather than the $\sim 10^3$ -yr lifetimes expected from simple 10 km s^{-1} expansion. Two possible explanations were offered by the authors: Either these regions are the ionized cores of dense stellar winds (E-type H II regions), or else ultracompact H II regions reform repeatedly as a result of luminosity oscillations [described by Yorke & Krügel (201)] during late star formation phases. Habing & Israel (62) noted the same discrepancy in observed and predicted lifetimes of ultracompact H II regions and H₂O masers. Rather than searching for a cause for the slower expansions of ultracompact H II regions, however, we should more carefully estimate their lifetimes, taking into consideration that some of these ultracompact sources are ionized by the Balmer continuum photons of stars with $M \simeq 10 M_{\odot}$ (as discussed above). Ultracompact H II regions should be more numerous than is predicted by simple expansion models of H II regions that consider Ly α ionization only.

3.3 *The Expansion of H II Regions—The Champagne Phase*

Numerical evolution calculations of H II regions in large-scale, non-uniform environments under a variety of different conditions have been performed by a number of investigators in one-dimensional (14, 167, 170, 183) and two-dimensional (22, 23, 141, 142, 171, 172, 199, 200, 202) geometry. Generally speaking, these calculations show that the S-type H II regions expand preferentially toward directions of decreasing density and that the ionized gas can attain supersonic velocities, in contrast to predictions of the classical expansion theory. In a clumpy medium, one can expect the weak D-type I-front with its preceding shock to pass around the more dense clumps of neutral material, compressing them and thus resulting in embedded neutral globules and elephant-trunk configurations [see the similarity solutions by Marsh (104), and the hydrodynamic results in one dimension by Tenorio-Tagle (165) and two dimensions by Sandford

et al. (141, 142)]. Another explanation for some long-lived neutral inclusions and bright rims in H II regions has been offered by Tenorio-Tagle (166), who calculates the collisions of different types of I-fronts in interacting H II regions [see also Brand (25)].

Eventually the I-front of an expanding H II region within a molecular cloud reaches the cloud's edge and the champagne phase begins [see reviews by Tenorio-Tagle (169) and Lazareff (93)]. In the idealized numerical models of Tenorio-Tagle and coworkers (14, 22, 167, 170-172, 199, 200, 202), the molecular cloud's edge is assumed to be a constant-pressure contact discontinuity (cd), where temperature and density change by several orders of magnitude. Depending on the depth of the ionizing source in the cloud, either a weak D-type or R-type I-front (R and D cases) crosses the cd edge. In both cases a weak R-front quickly moves through the low-density intercloud gas, and a pressure difference of several orders of magnitude is left behind at the cloud's former edge. The 10^4 -K high-density material expands outward from the cloud as a rarefaction wave travels inward through the H II region. At first, the weak D-type I-front still moving into the molecular clouds takes no notice of this expansion, but as the rarefaction wave crosses past the source, the supply of ionizing photons at the D-front increases with time and the I-front, with its leading shock, becomes faster [cf. Bedijn & Tenorio-Tagle (14)]. The resulting configuration is a blister-type H II region [cf. Israel (73, 74)], which is ionization bounded on the molecular cloud side and density bounded on the side of outward champagne flow (see Figure 3). The density distribution of ionized gas is roughly fan shaped and decreases approximately exponentially away from the cloud, whereas the velocity increases to several times the sound speed. Because line emission is strongly density dependent (it often varies as n^2), line profiles are often dominated by the denser low-velocity gas [Yorke et al. (203)].

The initial density discontinuity at the cloud's edge is not a crucial assumption. Soon after the I-front crosses the cloud's edge, the density gradient becomes finite; the "edge" is smeared out significantly while the expanding gas is still subsonic. Numerical models by Welter (188) and analytic considerations by Mazurek (107) show that champagne-type supersonic flows occur for modest density gradients.

Compared with the one-dimensional calculations, the two-dimensional champagne flow calculations were able to consider a greater variety of physical situations at the cost of more simplified physics. The R and D cases of Tenorio-Tagle (167) were recalculated in two-dimensional axial symmetry by Bodenheimer et al. (22) and Yorke et al. (202). A single example is shown in Figure 3. Double champagne flows in sheetlike clouds were also considered [(22, 202), Tenorio-Tagle et al. (172)], which result

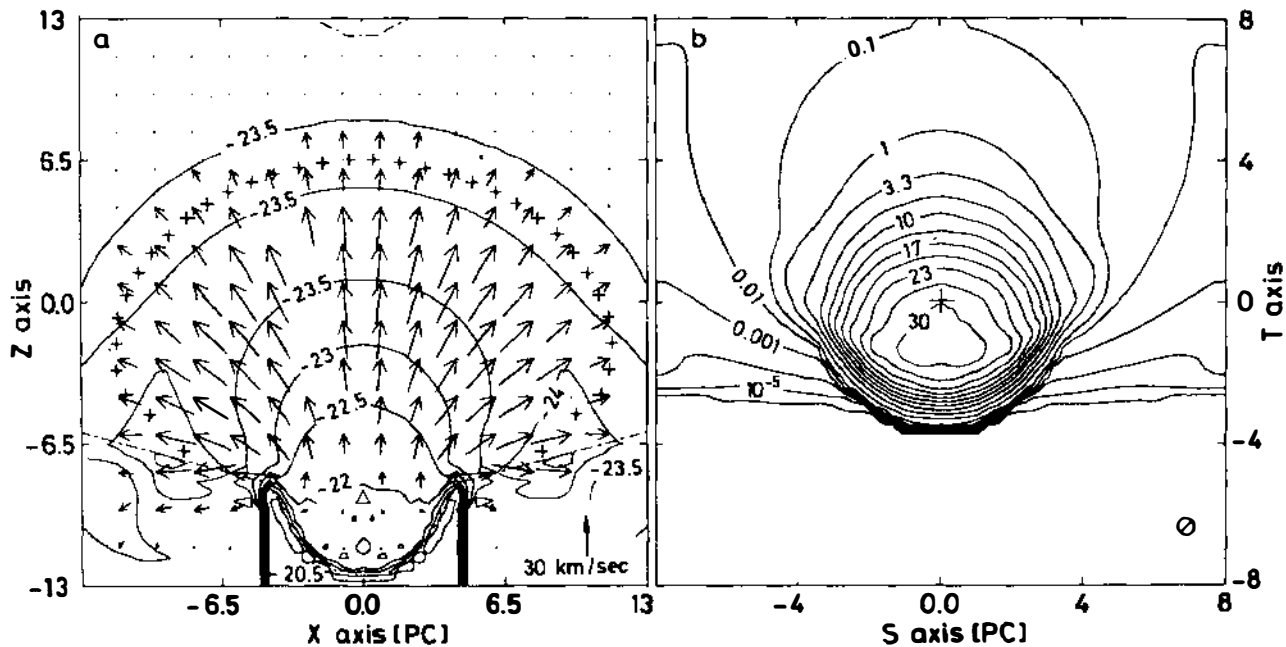


Figure 3 (a) Isodensity contour lines and velocity arrows in the meridional plane show the champagne flow in cylindrical symmetry at $t = 6.6 \times 10^5$ yr after an O star (7.6×10^{48} Lyc photons s^{-1}) turns on inside of a molecular cloud about one Strömgen radius from its edge. Contour levels are labeled with values for $\log \rho$ (cgs units); the H II region boundary is given by the dashed-dotted line. Arrows show the magnitude and direction of the gas velocity at selected points (tips of arrows); the velocity scale for an arrow of unit length is given in the lower right corner. The triangle denotes the position of the ionizing source. Crosses mark the positions of Lagrangian tracers originally at the cloud's edge. (b) The calculated radio map at $\lambda = 11$ cm of the champagne blister displayed in (a) is shown as seen by an "observer" in the equatorial plane. The projected position of the star is indicated by the cross. Contour levels are labeled by the surface brightness in units $f_0 = 10^{-18}$ erg s^{-1} cm^{-2} Hz^{-1} . The assumed beam size is indicated at the lower right. Contour levels are spaced linearly close to the star and logarithmically for levels less than f_0 [from Yorke et al. (202)].

in low-velocity ($\approx 30 \text{ km s}^{-1}$) bipolar flows. The interaction of champagne flows with embedded globules was studied [(22, 172), Yorke et al. (199, 200, 202)], although in this case the radial sector approximation is problematical as a result of the sharp shadows cast by the globules. A more realistic treatment, which allows for ionization on the globules' backsides by Lyc recombination photons in the champagne flow and by scattered radiation [cf. Sandford et al. (141, 142)], is required. The ionization of molecular clouds and the associated champagne flows due to stars located outside molecular clouds and moving relative to the cloud boundary (run-away O stars, blue stragglers) were also considered (172, 199). Calculations of champagne flows in massive collapsing and rotating clouds (199, 200) demonstrate that the champagne effect is able to ionize and disperse self-gravitating clouds even when the escape velocity at the boundary is greater than the isothermal sound speed of the ionized gas.

Taking into account the calculations of the line formation that takes place during the champagne phase [Yorke et al. (203)], we can summarize the main consequences of this phase as follows:

1. There is an approximate exponential density drop in the ionizing gas that streams away from the neutral cloud. H II blisters at the edges of clouds result.
2. The velocity of the ionized gas increases with increasing distance from the cloud and can attain values in excess of 30 km s^{-1} . The integrated Doppler-shifted velocity of the ionized gas is only modest, however [$\approx 5 \text{ km s}^{-1}$ away from the cloud (the exact value depends on geometric orientation)].
3. Complex velocity structure in lines (multiple components separated by up to 40 km s^{-1} , line broadening, and line asymmetries) could be present at various positions within a nebulae, with a tendency for greater complexity in the low-density, density-bounded periphery of the flow. The complexity of line profiles is also a function of beam size and orientation.
4. The champagne phase produces a low-density, extended H II region. A large percentage of ionizing photons can leak out of the density-bounded surface and maintain partial ionization of the warm intercloud medium. When these photons interact with neighboring molecular clouds, long-lived bright rims are produced.
5. The champagne phenomenon is an important mechanism for the input of kinetic energy into the interstellar medium. Several 10^{50} erg can be imparted to ionized gas by a single O5 star.
6. Molecular clouds can be partially or totally disrupted during the champagne phase. A single O5 star interacting with an isolated molecular cloud can initiate cloud disruption at the rate of $10^{-2 \pm 0.5} M_{\odot} \text{ yr}^{-1}$,

depending on individual circumstances. Self-gravity does not significantly alter the disruption rate. Similar estimates of molecular cloud erosion rates have been suggested by Whitworth (190a), and thus type-II molecular clouds should have life-times of the order of 10^7 yr.

7. The champagne phenomenon provides a natural explanation for the rather "sudden" transition from the compact H II region stage to the extended, low-density stage as inferred from the statistics of sizes and mean electron densities of H II regions [Harten & Felli (64)].

3.4 *The Recombination Phase—The Fate of an Evolving OB Association*

Beltrametti et al. (15) and Tenorio-Tagle et al. (171) have followed the one-dimensional and two-dimensional evolution of H II regions by taking an evolving OB association [source L2 (initially with 2×10^{51} Lyc photons s^{-1})] as an ionizing point source in a constant-density medium or inside of a giant molecular cloud near its edge. They find that recombination resulting from the decreasing ionizing flux can lead to large ($R \sim 40\text{--}100$ pc), thick ($\Delta R \gtrsim 10$ pc) neutral shells expanding at velocities of $10\text{--}30$ km s^{-1} . This phase can be inhibited if the ambient density is sufficiently high ($\gtrsim 400$ cm^{-3}). For lower densities the expanding neutral shell can be ionized prior to the first supernova explosions. Reinforced rarefaction of the ionized gas gives the H II region a ringlike appearance, regardless of whether a neutral shell was present or whether the H II region previously experienced the champagne phase. It should be noted that the usual interpretation of H II rings invokes stellar winds to create cavities [cf. McCray (109)].

Bodenheimer et al. (23) use the same ionizing source in a different environment to study the effects of supernova explosions in an H II region that has evolved in a stratified galactic disk with parameters (scale height and density) typical of a 10-kpc galactocentric radius. Prior to the first explosions, the recession of the I-front led to a large expanding ring of neutral gas of 800 pc diameter and 50–100 pc thickness. After some 200 supernova explosions, each with an energy of 10^{51} erg, rather modest shells were produced. The energetic "supershells" ($10^{52.4}\text{--}10^{54}$ erg) observed and discussed by Heiles (65, 66) could not be reproduced. In the calculations described above, W-R star formation and stellar winds were not considered.

Bruhweiler et al. (26) and Tomisaka et al. (178) considered the combined effects of many stellar winds of an OB association in creating cavities prior to the supernova explosions and were also able to explain supershells of more modest energy. Prior H II region evolution was not considered. Tenorio-Tagle (168) has suggested that Heiles' most energetic supershells

could be explained by the collisions of high-velocity clouds with the galactic disk. Such collisions could also initiate star formation.

4. CONFRONTATION OF THEORY AND OBSERVATIONS—PROSPECTS FOR THE FUTURE

The interpretation of all available observational data allows one to construct “models” of individual sources. The piecing together of these interpretive models into an evolutionary sequence is not a trivial task. Conceivably, there may be more than one avenue of evolution. Theoretical evolution models, as described in Section 3, are by necessity simplistic and cannot compete with the complexity of reality.

4.1 *Observations of Ultracompact H II Regions*

Radio and infrared observations of high spatial and spectral resolution can now discern the earliest stages in the evolution of an H II region. The detection of the Becklin-Neugebauer object (BN) at 15 and 23 GHz [Moran et al. (121)] with a spectral index of ~ 2 confirmed in detail what was suspected after Grasdalen's (61) discovery of Br α : BN is an ultracompact ($\sim 3 \times 10^{14}$ cm) H II region, optically thick in radio up to about 40 GHz, and is a member of a growing list of such objects [see Habing & Israel (62) for a definition of ultracompactness, and (9, 43, 120, 150, 177, 183, 193) for recent additions and further references]. Thompson (176) compares the emission measure versus luminosity (assuming optically thin IR hydrogen lines) for 17 of these objects with his tabulated values for Kurucz (81) atmospheres and finds that the observed points generally lie between the Balmer and Lyc continuum curves. This result demonstrates the adequacy of Balmer continuum photons in explaining the “excess” IR hydrogen lines [as suggested by Simon et al. (150)], but it raises the question as to why these lines are not even stronger, which would bring the observed points closer to the Balmer continuum curve. The most obvious explanation—namely, optically thick lines that also invalidate the assumptions of case B recombination theory [cf. Osterbrock (127)]—does have observational support, but as discussed by Thompson, other effects may also be operative, such as dust absorption, density boundedness, and inadequacies of the model atmospheres. More detailed interpretive models that include full radiative transfer effects are necessary for definitive predictions. Accreting flows, with their modifications of the ionizing flux (contributions from an accretion shock, inflated photospheres), cannot be ruled out completely, except for a few sources such as the bipolar nebula S106 (e.g. 9, 10, 45, 153, 159).

More sophisticated hydrodynamic evolutionary models than those dis-

cussed in Section 3, linking the ultracompact H II phase to the exciting star's formation, are conspicuously needed. High-spatial-resolution sub-millimeter and millimeter mapping will help set the direction.

4.2 *The Appearance of H II Blisters and Champagne Flow*

Many discrepancies between the observed morphology and structure of emission nebulae and the predictions of the classical theory (i.e. observed nonsphericity, nonuniform density and radial velocity distributions, their density boundedness, supersonic velocities with line asymmetries and splitting) led to a new class of interpretive models. Perhaps the best known of these is Zuckerman's (205) suggestion that the Orion Nebula is a protrusion off the front edge of the dense molecular cloud associated with the KL nebula. The champagne evolutionary model (see Section 3) provided the explanation of how such protrusions can form from compact H II regions located in molecular clouds and made definitive observable predictions of density and velocity structure of the ionized gas and its relation to the molecular cloud.

It was soon clear that a large majority of optical H II regions are located at the edges of molecular clouds [Israel (73, 74), Blitz et al. (18)] from which the ionized material appears to be streaming away [see also Fich et al. (50)]. Theoretical radio continuum [Icke (70, 71), Icke et al. (72)] and line emission [Rubin (139), Aannestad & Emery (1)] of H II regions in assumed stratified media can qualitatively reproduce many of the observed features of such H II blisters to the extent that observational data are available. Velocity splitting of up to 50 km s^{-1} was also predicted [Icke (70)] by using assumed velocity distributions. Yorke et al. (202, 203) have taken a different approach, calculating radio maps (202) and line profiles (203) from two-dimensional hydrodynamical models. The resemblance of their radio maps to those of Icke and Icke et al. is not surprising, because the hydrodynamical results predict an approximate exponential decrease of density of ionized gas from the molecular cloud.

The line profile calculations of Yorke et al. (203) display greater complexity (multiple velocity components separated by up to 40 km s^{-1} , broadening and asymmetries that vary across the model nebulae) than those of Icke (70). Observed line profile complexity of this nature is often attributed to stellar winds for no better reason than the presence of supersonic velocities, which supposedly cannot occur in H II region expansion theory.

A detailed discussion of optical H II regions, which because of their overall morphological appearance and line profile structures can be interpreted as blisters in the champagne phase, would be too long to include in the present review. Icke et al. (72) give modeling parameters for 10 of

them (S255, S257, S271, S156, S125, S184, S235, S206, W3A, and Orion A). Certainly a large number of well-known sources can be added to this list (e.g. S115, S236, S90, S157, S158, S159, M8, Orion B, etc.), some of which were discussed at the Penticton conference (137).

As a final remark, we note that present evolutionary models of H II regions include either the effects of stellar outflows or of champagne flows, but not both. Clearly both will be important during the course of evolution of H II regions around young hot stars, especially when evolving OB associations are considered. Sources such as 30 Dor remind us of how complex these interactions—including multiple supernova explosions—can really be.

ACKNOWLEDGMENTS

This work was supported under DFG grants Yo 5/4-1 and Yo 5/3-1. Many invigorating discussions with colleagues at Lick Observatory and participants at the 1984 Santa Cruz Workshop on Active Galaxies and QSOs proved to be very useful. The author especially thanks Drs. Bodenheimer, O'Dell, Netzer, and Tenorio-Tagle. Many thanks also to Dr. Péquignot for his organization of the Paris Workshop on Model Nebulae and the opportunity for many detailed discussions on the present subject. The efforts by colleagues and technical staff at the University Observatory in Göttingen, who helped with figures, typing, proofreading, discussions, and moral support, are greatly appreciated.

Literature Cited

1. Aannestad, P. A., Emery, R. J. 1985. *Astron. Astrophys.* 145: 347–52
2. Aldrovandi, S. M. V., Contini, M. 1985. *Astron. Astrophys.* 149: 109–17
3. Allen, C. W. 1973. *Astrophysical Quantities*. London: Athlone. 310 pp. 3rd ed.
4. Aller, L. H. 1984. *Physics of Thermal Gaseous Nebulae*. Dordrecht: Reidel. 350 pp.
5. Arnaud, M. 1986. See Ref. 131. In press
6. Arnaud, M., Rothenflug, R. 1985. *Astron. Astrophys. Suppl.* 60: 425–51
7. Axford, W. I. 1961. *Philos. Trans. R. Soc. London Ser. A* 253: 301–33
8. Bally, J., Lada, C. J. 1983. *Ap. J.* 265: 824–47
9. Bally, J., Predmore, R. 1983. *Ap. J.* 265: 778–90
10. Bally, J., Snell, R. L., Predmore, R. 1983. *Ap. J.* 272: 154–62
11. Baschek, B., Kudritzki, R. P., Scholz, M., Simon, K. P. 1982. *Astron. Astrophys.* 108: 387–405
12. Baschek, B., Scholz, M. 1982. In *Landolt-Börnstein, Numerical Data and Functional Relationships in Science and Technology*, ed. H. H. Voigt, K. Schaiffers, Vol. VI/2B, Sect. 4.3. Heidelberg: Springer
13. Bastien, P., Batrla, W., Henkel, C., Pauls, T., Walmsley, C. M., Wilson, T. L. 1985. *Astron. Astrophys.* 146: 86–94
14. Bedijn, P. J., Tenorio-Tagle, G. 1981. *Astron. Astrophys.* 98: 85–91
15. Beltrametti, M., Tenorio-Tagle, G., Yorke, H. W. 1982. *Astron. Astrophys.* 112: 1–10
16. Bertout, C. 1984. *Rep. Prog. Phys.* 47: 111–74
17. Bertout, C., Yorke, H. W. 1978. See Ref. 57, pp. 648–89
18. Blitz, L., Fich, M., Stark, A. A. 1982. See Ref. 137, pp. 209–12
19. Blitz, L., Shu, F. H. 1980. *Ap. J.* 238: 148–57

20. Bochkarev, N. G., Lozinskaya, T. A. 1985. *Sov. Astron. AJ* 29: 60–64
21. Bodenheimer, P. 1981. See Ref. 163, pp. 5–26
22. Bodenheimer, P., Tenorio-Tagle, G., Yorke, H. W. 1979. *Ap. J.* 233: 85–96
23. Bodenheimer, P., Yorke, H. W., Tenorio-Tagle, G., Beltrametti, M. 1983. See Ref. 35, pp. 399–404
24. Borsenberger, J., Stasinska, G. 1982. *Astron. Astrophys.* 106: 158–62
25. Brand, P. W. J. L. 1981. *MNRAS* 197: 217–33
26. Bruhweiler, F. C., Gull, T. R., Kafatos, M., Sofia, S. 1980. *Ap. J. Lett.* 238: L27–30
27. Cassinelli, J. P. 1979. *Ann. Rev. Astron. Astrophys.* 17: 275–308
28. Chiosi, C. 1981. See Ref. 40, pp. 27–48
29. Chiosi, C. 1982. See Ref. 38, pp. 323–41
30. Chiosi, C., Maeder, A. 1986. *Ann. Rev. Astron. Astrophys.* 24: 329–75
31. Chu, Y.-H., Treffers, R. R., Kwitter, K. B. 1983. *Ap. J. Suppl.* 53: 937–44
32. Compte, C., Monnet, G. 1974. *Astron. Astrophys.* 33: 161–76
33. Conti, P. S. 1978. *Ann. Rev. Astron. Astrophys.* 16: 371–92
34. Cox, J. P., Giuli, R. T. 1968. *Principles of Stellar Structure*, Vol. 2. New York: Gordon & Breach. 758 pp.
35. Danziger, J., Gorenstein, P., eds. 1983. *Supernova Remnants and Their X-Ray Emission*, IAU Symp. No. 101. Dordrecht: Reidel. 614 pp.
36. deJager, C. 1980. *The Brightest Stars*. Dordrecht: Reidel. 458 pp.
37. deLoore, C. 1982. See Ref. 38, pp. 343–58
38. deLoore, C. W. H., Willis, A. J., eds. 1982. *Wolf-Rayet Stars: Observations, Physics, Evolution*, IAU Symp. No. 99. Dordrecht: Reidel. 618 pp.
39. Dickey, J. M., ed. 1981. *The Phases of the Interstellar Medium*. Green Bank, W. Va.: NRAO. 206 pp.
40. D’Odorico, S., Baade, D., Kjær, K., eds. 1981. *The Most Massive Stars*. Garching: ESO. 365 pp.
41. Draine, B. T. 1980. *Ap. J.* 241: 1021–38
42. Draine, B. T. 1983. *Ap. J.* 270: 519–36
43. Dreher, J. W., Johnston, K. J., Welch, W. J., Walker, R. C. 1984. *Ap. J.* 283: 632–39
44. Dupree, A. K. 1986. *Ann. Rev. Astron. Astrophys.* 24: 377–420
45. Dyson, J. E. 1983. *Astron. Astrophys.* 124: 77–83
46. Dyson, J. E. 1985. *Astrophys. Space Sci.* 106: 181–97
47. Elsässer, H. 1983. *Mitt. Astron. Ges.* 60: 59–72
48. Evans, I. N., Dopita, M. A. 1985. *Ap. J. Suppl.* 58: 125–42
49. Ferland, G., Netzer, H. 1983. *Ap. J.* 264: 105–13
50. Fich, M., Treffers, R. R., Blitz, L. 1982. See Ref. 137, pp. 201–8
51. Flower, D. R., ed. 1983. *Planetary Nebulae*, IAU Symp. No. 103. Dordrecht: Reidel. 557 pp.
52. Friedjung, M., Viotti, R., eds. 1982. *The Nature of Symbiotic Stars*, IAU Colloq. No. 70. Dordrecht: Reidel. 310 pp.
53. Gail, H.-P., Sedlmayr, E. 1979. *Astron. Astrophys.* 76: 158–67
54. Gail, H.-P., Sedlmayr, E. 1979. *Astron. Astrophys.* 77: 165–77
55. Garlick, A. R. 1978. *Astron. Astrophys.* 68: 113–21
56. Gautier, T. N. III, Fink, U., Treffers, R. R., Larson, H. P. 1976. *Ap. J. Lett.* 207: L129–33
57. Gehrels, T., ed. 1978. *Protostars and Planets*. Tucson: Univ. Ariz. Press. 756 pp.
58. Genzel, R., Downes, D. 1983. In *Highlights of Astronomy*, ed. R. M. West, 6: 489–706. Dordrecht: Reidel. 817 pp.
59. Goldsworthy, F. A. 1961. *Philos. Trans. R. Soc. London Ser. A* 253: 277–300
60. Goldsworthy, F. A. 1984. *IMA J. Appl. Math.* 32: 147–73
61. Grasdalen, G. L. 1976. *Ap. J. Lett.* 205: L83–85
62. Habing, H. J., Israel, F. P. 1979. *Ann. Rev. Astron. Astrophys.* 17: 345–85
63. Harrington, J. P. 1977. *MNRAS* 179: 63–79
64. Harten, R. H., Felli, M. 1982. See Ref. 137, pp. 25–30
65. Heiles, C. 1979. *Ap. J.* 229: 533–44
66. Heiles, C. 1983. See Ref. 35, pp. 367–72
67. Heiles, C., Chu, Y.-H., Troland, T. H. 1981. *Ap. J. Lett.* 247: L77–80
68. Hjellming, R. M. 1966. *Ap. J.* 143: 420–51
69. Ho, P. T. P., Barrett, A. H. 1978. *Ap. J. Lett.* 224: L23–26
70. Icke, V. 1979. *Astron. Astrophys.* 78: 352–61
71. Icke, V. 1981. *Ap. J. Suppl.* 45: 585–602
72. Icke, V., Gatley, I., Israel, F. P. 1980. *Ap. J.* 236: 808–22
73. Israel, F. P. 1976. PhD thesis. Univ. Leiden, Neth.
74. Israel, F. P. 1978. *Astron. Astrophys.* 70: 769–75
75. Kahane, C., Guilloteau, S., Lucas, R. 1985. *Astron. Astrophys.* 146: 325–36

76. Kahn, F. D. 1954. *Bull. Astron. Inst. Neth.* 12: 187–200
77. Kaler, J. B. 1985. *Ann. Rev. Astron. Astrophys.* 23: 89–117
78. Köppen, J. 1979. *Astron. Astrophys. Suppl.* 35: 111–27
79. Köppen, J., Schmid-Burgk, J., Scholz, M. 1983. *Astron. Astrophys.* 118: 203–5
80. Krolik, J. H., Smith, H. A. 1981. *Ap. J.* 249: 628–36
81. Kurucz, R. L. 1979. *Ap. J. Suppl.* 40: 1–340
82. Kurucz, R. L., Peytremann, E., Avrett, E. H. 1974. *Blanketed Model Atmospheres*. Washington, DC: Smithsonian Inst. 186 pp.
83. Kutner, M. L., Evans, N. J. II, Tucker, K. D. 1976. *Ap. J.* 209: 452–61
84. Kwan, J., Scoville, N. Z. 1976. *Ap. J. Lett.* 210: L39–43
85. Lada, C. J. 1985. *Ann. Rev. Astron. Astrophys.* 23: 267–317
86. Landau, L. D., Lifshitz, E. M. 1963. *Electrodynamics of Continuous Media*. New York: Pergamon. 417 pp, 2nd ed.
87. Langer, N., El Eid, M. F., Fricke, K. J. 1985. *Astron. Astrophys.* 145: 179–91
88. Larson, R. B. 1972. *MNRAS* 157: 121–45
89. Larson, R. B. 1973. *Ann. Rev. Astron. Astrophys.* 11: 219–38
90. Larson, R. B. 1981. *MNRAS* 194: 809–29
91. Lasker, B. M. 1966. *Ap. J.* 143: 700–21
92. Lasker, B. M. 1966. *Ap. J.* 146: 471–79
93. Lazareff, B. 1981. In *Mécanismes de Production d'Énergie dans le Milieu Interstellaire*, ed. J. P. Sivan, pp. 141–73. Marseille: Lab. Astron. Spat. du CNRS. 284 pp.
94. Leiknes, J., Havnes, O. 1984. *Astron. Astrophys. Suppl.* 57: 263–74
95. Maciel, W. J., Pottasch, S. R. 1982. *Astron. Astrophys.* 106: 1–3
96. Maeder, A. 1981. See Ref. 40, pp. 173–89
97. Maeder, A. 1984. See Ref. 98, pp. 299–319
98. Maeder, A., Renzini, A., eds. 1984. *Observational Tests of the Stellar Evolution Theory, IAU Symp. No. 105*. Dordrecht: Reidel. 590 pp.
99. Mallik, D. C. V. 1975. *Ap. J.* 197: 355–63
100. Manfroid, J. 1976. *Astron. Astrophys.* 46: 31–39
101. Manfroid, J. 1976. *Astrophys. Space Sci.* 41: 39–56
102. Manfroid, J. 1977. *Astron. Astrophys.* 58: 295–96
103. Manfroid, J. 1977. *Astron. Astrophys.* 61: 437–42
104. Marsh, M. C. 1970. *MNRAS* 147: 95–114
105. Mathews, W. G. 1965. *Ap. J.* 142: 1120–40
106. Mathews, W. G., O'Dell, C. R. 1969. *Ann. Rev. Astron. Astrophys.* 7: 67–98
107. Mazurek, T. J. 1982. See Ref. 137, pp. 61–66
108. McCarroll, R., Valiron, P., Opradolce, L. 1983. See Ref. 51, pp. 187–97
109. McCray, R. 1983. In *Highlights of Astronomy*, ed. R. M. West, 6: 565–79. Dordrecht: Reidel. 817 pp.
110. McCray, R., Snow, T. P. Jr. 1979. *Ann. Rev. Astron. Astrophys.* 17: 213–40
111. Mendoza, C. 1983. See Ref. 51, pp. 143–72
112. Mezger, P. G. 1978. *Astron. Astrophys.* 70: 565–74
113. Mihalas, D. 1972. *NCAR Tech. Note NCAR-TN/STR-76*. Boulder, Colo: Natl. Cent. Atmos. Res.
114. Mihalas, D. 1978. *Stellar Atmospheres*. San Francisco: Freeman. 632 pp. 2nd ed.
115. Mihalas, D. 1985. *J. Comput. Phys.* 57: 1–25
116. Misner, C. W., Thorne, K. S., Wheeler, J. A. 1973. *Gravitation*. San Francisco: Freeman. 1279 pp.
117. Mitchell, G. F., Deveau, T. J. 1983. *Ap. J.* 266: 646–61
118. Mitchell, G. F., Watt, G. D. 1985. *Astron. Astrophys.* 151: 120–31
119. Moorwood, A. F. M., Feuerbach, B. 1976. In *Solid State Astrophysics*, ed. N. C. Wickramasinghe, D. J. Morgan, pp. 179–89. Dordrecht: Reidel. 314 pp.
120. Moorwood, A. F. M., Salinari, P. 1983. *Astron. Astrophys.* 125: 342–54
121. Moran, J. M., Garay, G., Reid, M. J., Genzel, R., Wright, M. C. H., Plambeck, R. L. 1983. *Ap. J. Lett.* 271: L31–34
122. Mouschovias, T. C. 1981. See Ref. 163, pp. 27–62
123. Myers, P. C., Benson, P. J. 1983. *Ap. J.* 266: 309–20
124. Nussbaumer, H. 1986. See Ref. 131. In press
125. Nussbaumer, H., Storey, P. J. 1983. *Astron. Astrophys.* 126: 75–79
126. Nussbaumer, H., Storey, P. J. 1984. *Astron. Astrophys. Suppl.* 56: 293–312
127. Osterbrock, D. E. 1974. *Astrophysics of Gaseous Nebulae*. San Francisco: Freeman. 251 pp.
128. Panagia, N. 1973. *Astron. J.* 78: 929–34
129. Panagia, N., Felli, M. 1975. *Astron. Astrophys.* 39: 1–5

130. Pascoli, G. 1985. *Astron. Astrophys.* 147: 257-64
131. Péquignot, D., ed. 1986. *Workshop on Model Nebulae, Paris, 1985*. In press
132. Prasad, S. S., Huntress, W. T. 1980. *Ap. J. Suppl.* 43: 1-35
133. Prasad, S. S., Huntress, W. T. 1982. *Ap. J.* 260: 590-98
134. Pudritz, R. E. 1985. *Ap. J.* 293: 216-29
135. Pudritz, R. E., Norman, C. A. 1983. *Ap. J.* 274: 677-97
136. Richtmyer, R. D., Morton, K. W. 1967. *Difference Methods for Initial-Value Problems*. New York: Wiley. 405 pp. 2nd ed.
137. Roger, R. S., Dewdney, P. E., eds. 1982. *Regions of Recent Star Formation*. Dordrecht: Reidel. 496 pp.
138. Rozyczka, M., Tenorio-Tagle, G. 1985. *Astron. Astrophys.* 147: 209-19
139. Rubin, R. H. 1984. *Ap. J.* 287: 653-64
140. Rubin, R. H. 1985. *Ap. J. Suppl.* 57: 349-87
141. Sandford, M. T. II, Whitaker, R. W., Klein, R. I. 1982. *Ap. J.* 260: 183-201
142. Sandford, M. T. II, Whitaker, R. W., Klein, R. I. 1984. *Ap. J.* 282: 178-90
143. Scoville, N. Z. 1983. See Ref. 190b, pp. 1-14
144. Deleted in proof
145. Scoville, N. Z., Hersh, K. 1979. *Ap. J.* 229: 578-82
146. Shaver, P. A., McGee, R. X., Newton, L. M., Danks, A. C., Pottasch, S. R. 1983. *MNRAS* 204: 53-112
147. Shklovskij, I. S. 1956. *Astron. Zh.* 33: 315-29
148. Shull, J. M. 1982. See Ref. 137, pp. 91-105
149. Shull, J. M., van Steenberg, M. 1982. *Ap. J. Suppl.* 48: 95-107
150. Simon, M., Felli, M., Cassar, L., Fischer, J., Massi, M. 1983. *Ap. J.* 266: 623-45
151. Simon, M., Rhigini-Cohen, G., Fischer, J., Cassar, L. 1981. *Ap. J.* 251: 552-56
152. Snell, R. L., Scoville, N. Z., Sanders, D. B., Erickson, N. R. 1985. *Ap. J.* 284: 176-93
153. Solf, J., Carsenty, U. 1982. *Astron. Astrophys.* 113: 142-49
154. Solomon, P. M., Sanders, D. B. 1980. In *Giant Molecular Clouds in the Galaxy*, ed. P. M. Solomon, M. G. Edmunds, pp. 41-73. Oxford: Pergamon. 344 pp.
155. Deleted in proof
156. Spitzer, L. Jr. 1978. *Physical Processes in the Interstellar Medium*. New York: Wiley. 318 pp.
157. Spitzer, L. Jr., Savedoff, M. P. 1950. *Ap. J.* 111: 593-608
158. Stasinska, G. 1982. *Astron. Astrophys. Suppl.* 48: 299-304
159. Staude, H. J., Lenzen, R., Dyck, H. M., Schmidt, G. D. 1982. *Ap. J.* 255: 95-102
160. Stenholm, L. G. 1980. *Astron. Astrophys. Suppl.* 42: 23-41
161. Storey, P. J. 1983. See Ref. 51, pp. 199-209
162. Strömgren, B. 1939. *Ap. J.* 89: 526-54
163. Sugimoto, D., Lamb, D. Q., Schramm, D. N., eds. 1981. *Fundamental Problems in the Theory of Stellar Evolution, IAU Symp. No. 93*. Dordrecht: Reidel. 347 pp.
164. Tenorio-Tagle, G. 1976. *Astron. Astrophys.* 53: 411-17
165. Tenorio-Tagle, G. 1977. *Astron. Astrophys.* 54: 517-24
166. Tenorio-Tagle, G. 1977. *Astron. Astrophys.* 61: 189-94
167. Tenorio-Tagle, G. 1979. *Astron. Astrophys.* 71: 59-67
168. Tenorio-Tagle, G. 1981. *Astron. Astrophys.* 94: 338-44
169. Tenorio-Tagle, G. 1982. See Ref. 137, pp. 1-14
170. Tenorio-Tagle, G., Bedijn, P. J. 1981. *Astron. Astrophys.* 99: 305-10
171. Tenorio-Tagle, G., Beltrametti, M., Bodenheimer, P., Yorke, H. W. 1982. *Astron. Astrophys.* 112: 104-10
172. Tenorio-Tagle, G., Yorke, H. W., Bodenheimer, P. 1979. *Astron. Astrophys.* 80: 110-18
173. Terlevich, R., Melnik, J. 1985. *MNRAS* 213: 841-56
174. Terzian, Y., ed. 1968. *Interstellar Ionized Hydrogen*. New York: Benjamin. 774 pp.
175. Thaddeus, P., Dame, T. M. 1983. See Ref. 190b, pp. 15-26
176. Thompson, R. I. 1984. *Ap. J.* 283: 165-68
177. Thompson, R. I., Thronson, H. A. 1983. *Ap. J.* 266: 614-22
178. Tomisaka, K., Habe, A., Ikeuchi, S. 1981. *Astrophys. Space Sci.* 78: 273-85
179. Torbett, M. V. 1984. *Ap. J.* 278: 318-25
180. Torrelles, J. M., Rodriguez, L. F., Canto, J., Carral, P., Marciade, J., et al. 1983. *Ap. J.* 274: 214-30
181. Tscharnuter, W. M. 1981. See Ref. 163, pp. 105-6
182. Tscharnuter, W. M., Winkler, K.-H. 1979. *Comput. Phys. Commun.* 18: 171-99
183. Turner, B. E., Mathews, H. E. 1984. *Ap. J.* 277: 164-80

184. Vogel, S. N., Bieging, J. H., Plamböck, R. L., Welch, W. J., Wright, M. C. H. 1985. *Ap. J.* 296: 600–5
185. Watson, W. D. 1978. *Ann. Rev. Astron. Astrophys.* 16: 585–615
186. Watt, G. D. 1984. See Ref. 190b, pp. 133–45
187. Weaver, T. A., Zimmermann, G. B., Woosley, S. E. 1978. *Ap. J.* 225: 1021–29
188. Welter, G. L. 1980. *Ap. J.* 240: 514–23
189. Wcsemael, F. 1982. *Ap. J. Suppl.* 45: 171–257
- 190a. Whitworth, A. 1979. *MNRAS* 186: 59–67
- 190b. Wolstencroft, R. D., ed. 1983. *Edinburgh Star Formation Workshop, Occas. Rep. R. Obs. Edinburgh No. 13.* 227 pp.
191. Woodward, P. R. 1978. *Ann. Rev. Astron. Astrophys.* 16: 555–84
192. Wright, A. E., Barlow, M. J. 1975. *MNRAS* 170: 41–51
193. Wynn-Williams, G. 1982. *Ann. Rev. Astron. Astrophys.* 20: 587–618
194. Yorke, H. W. 1979. *Astron. Astrophys.* 80: 308–16
195. Yorke, H. W. 1980. *Astron. Astrophys.* 85: 215–20
196. Yorke, H. W. 1980. *Astron. Astrophys.* 86: 286–94
197. Yorke, H. W. 1981. In *Scientific Importance of High Angular Resolution of Infrared and Optical Wavelengths*, ed. M. H. Ulrich, K. Kjär, pp. 319–40. Garching: ESO. 443 pp.
198. Yorke, H. W. 1985. In *The Birth and Infancy of Stars, Les Houches Summer School, Sess. 41*, ed. R. Lucas, A. Omont, R. Stora, pp. 645–92. Amsterdam: North-Holland. 823 pp.
199. Yorke, H. W., Bodenheimer, P., Tenorio-Tagle, G. 1982. *Astron. Astrophys.* 108: 25–41
200. Yorke, H. W., Bodenheimer, P., Tenorio-Tagle, G. 1982. See Ref. 137, pp. 15–23
201. Yorke, H. W., Krügel, E. 1977. *Astron. Astrophys.* 54: 183–94
202. Yorke, H. W., Tenorio-Tagle, G., Bodenheimer, P. 1983. *Astron. Astrophys.* 127: 313–19
203. Yorke, H. W., Tenorio-Tagle, G., Bodenheimer, P. 1984. *Astron. Astrophys.* 138: 325–32
204. Zeippen, C. 1986. See Ref. 131. In press
205. Zuckerman, B. 1973. *Ap. J.* 183: 863–69
206. Zuckerman, B., Kuiper, T. B. H., Rodriguez-Kuiper, E. N. 1976. *Ap. J. Lett.* 209: L137–42



CONTENTS

A HALF-CENTURY OF ASTRONOMY, <i>A. E. Whitford</i>	1
THE QUIET SOLAR TRANSITION REGION, <i>John T. Mariska</i>	23
THE DYNAMICAL EVOLUTION OF H II REGIONS—Recent Theoretical Developments, <i>Harold W. Yorke</i>	49
MOLECULES IN STARS, <i>T. Tsuji</i>	89
MAXIMUM ENTROPY IMAGE RESTORATION IN ASTRONOMY, <i>Ramesh Narayan and Rajaram Nityananda</i>	127
EMISSION-LINE REGIONS OF ACTIVE GALAXIES AND QSOs, <i>Donald E. Osterbrock and William G. Mathews</i>	171
THE PHYSICS OF SUPERNOVA EXPLOSIONS, <i>S. E. Woosley and Thomas A. Weaver</i>	205
CHARGE-COUPLED DEVICES IN ASTRONOMY, <i>Craig D. Mackay</i>	255
RECENT PROGRESS IN THE UNDERSTANDING OF PULSARS, <i>J. H. Taylor and D. R. Stinebring</i>	285
THE EVOLUTION OF MASSIVE STARS WITH MASS LOSS, <i>Cesare Chiosi and André Maeder</i>	329
MASS LOSS FROM COOL STARS, <i>A. K. Dupree</i>	377
THE POPULATION CONCEPT, GLOBULAR CLUSTERS, SUBDWARFS, AGES, AND THE COLLAPSE OF THE GALAXY, <i>Allan Sandage</i>	421
GLOBAL STRUCTURE OF MAGNETIC FIELDS IN SPIRAL GALAXIES, <i>Yoshiaki Sofue, Mitsuaki Fujimoto, and Richard Wielebinski</i>	459
HIGH-RESOLUTION OPTICAL AND ULTRAVIOLET ABSORPTION-LINE STUDIES OF INTERSTELLAR GAS, <i>Lennox L. Cowie and Antoinette Songaila</i>	499
PULSAR TIMING AND GENERAL RELATIVITY, <i>D. C. Backer and R. W. Hellings</i>	537
STAR COUNTS AND GALACTIC STRUCTURE, <i>John N. Bahcall</i>	577
INDEXES	
Subject Index	613
Cumulative Index of Contributing Authors, Volumes 14–24	620
Cumulative Index of Chapter Titles, Volumes 14–24	622